D6.5 Dynamic link to hazard and resilience assessment

Deliverable number	**D6.5**
Deliverable title	**Dynamic link to hazard and resilience assessment**
Nature[1]	**R**
Dissemination Level [2]	**PU**
Author (email) Institution	**Enrique Herandez-Montes (emontes@ugr.es)** **UGR** **Luisa María Gil-Martín (mlgil@ugr.es)** **UGR**
Editor (email) Institution	**Dimitrios Vamvatsikos (divamva@mail.ntua.gr)** **NTUA**
Leading partner	**UGR**
Participating partners	**UGR, UNIPD, IUAV, NTUA**
Official submission date:	**14/12/2021**
Actual submission date:	**28/06/2022**

[1] **R**=Document, report; **DEM**=Demonstrator, pilot, prototype; **DEC**=website, patent fillings, videos, etc.; **OTHER**=other

[2] **PU**=Public, **CO**=Confidential, only for members of the consortium (including the Commission Services), **CI**=Classified, as referred to in Commission Decision 2001/844/EC

Modifications Index

Date	Version
28/03/2022	1st draft
12/05/2022	Internal Review
01/06/2022	2nd draft
28/06/2022	Internal Review and final draft

This work is a part of the HYPERION project. HYPERION has received funding from the European Union's Horizon 2020 research and innovation programme under grant agreement no 821054.

ACRONYMS AND ABBREVIATIONS

$AvgS_a$	Average Spectral Acceleration
C	Capacity
CC	Climate Change
CH	Cultural Heritage
D	Demand
DM	Damage Measure
EDP	Engineering Demand Parameter
HRAP	Holistic Risk Assessment Platform
IM	Intensity Measure
LS	Limit State
MHVM	Multi-Hazard Vulnerability Module
MSA	Multi-Stripe Analysis
PGA	Peak Ground Acceleration
R_{eq}	Equivalent ice thickness accumulated on a member
u_{10}	10-minute mean wind speed measured at 10m height from the ground

Table of Contents

Table of Figures

Table of Tables

Executive Summary

Deliverable D6.5 “Dynamic link to hazard and resilience assessment” documents the work performed in Task 6.5 “Linking degradation and damage information into a dynamic hazard and resilience assessment” during the period of months 22 to 30 of the project’s duration.

This deliverable focuses on the connection between hazard and resilience. The study of hazards includes modelling structures, degradation processes, and loadings. The study of resilience includes risk assessment and the cost of interventions. This deliverable works with observed infrastructure degradation or damage as well as with laboratory damage information. Additionally, due to the dynamic nature of the CC conditions, the information about the climate conditions of the CH area is regularly fed back into the risk assessment.

1 Introduction

1.1 Background

The deliverable D6.5 “Dynamic link to hazard and resilience assessment” is an important document. It establishes the framework that enables the information flow from CC to system risk/resilience.

All the information gathered within the D6.5 document will be encoded in software libraries that will enable a seamless integration of hazard simulators and vulnerability results into the HRAP of the system.

1.2 Scope and Objective

The main objective of D6.5 is to provide a methodology to feed the damage and degradation assessment results into the hazard and resilience models and data of WP5, to ensure a dynamic analysis. In a holistic approach D6.5 develops a methodology that generates values of degradation parameters from weather conditions. These values can be entered into WP5, to analyse risk.

In a first step the connection of the climate conditions and the evolution of the degradation of the building material is afforded, see Figure 1.

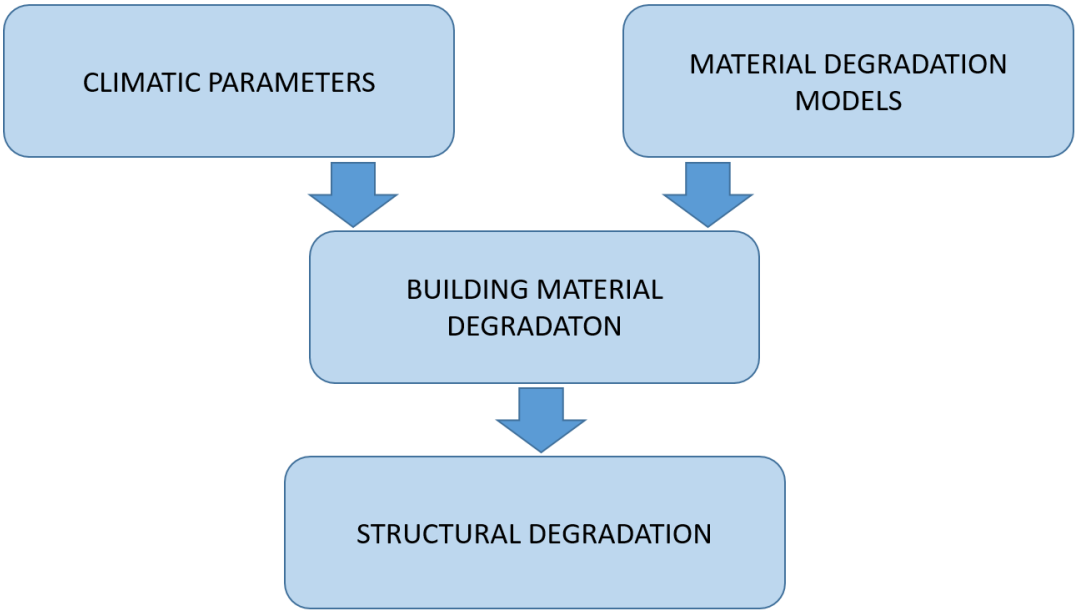

Figure 1. Prediction of the degradation

In a second step, the behaviour of the building material (mainly at laboratory level) is connected with the structural degradation (via observation). This will allow to obtain values of the structural degradation parameter from climatic conditions.

These degradation parameters (e.g. modulus of elasticity, depth of degradation, ...) are introduced into the structural model. The risk assessment is deduced from the study of the response of the structure using degraded and non-degraded materials.

The cost analysis is the last step prior to the decision of intervention if required, Figure 2.

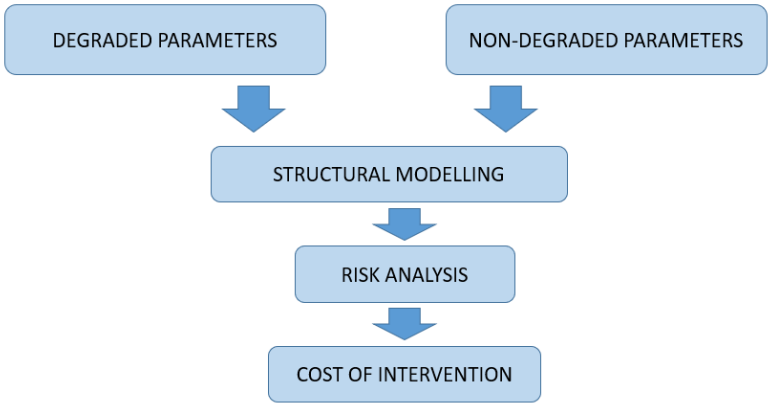

Figure 2. Cost analysis

Due to CC degradation processes can accelerate or slow, which alter the resilience of the CH and surrounding areas, which may require intervention.

1.3 Definitions

Deterioration evolution diagrams: Diagrams that relate the time of exposition and the unified climatic parameter with the observed degradation (observed engineering demand parameter).

Exposure model: it contains information about the assets at risk, their location, taxonomy, etc.

Fragility curve: function that provides the probability of exceeding a given limit state, or equivalently of being in a certain damage state or worse, given the intensity measure.

Hazard: stressors associated with a peril that may affect the normal activities of people and the integrity and functionality of CH and non-CH assets, including, for example, ground shaking for earthquakes or wind action for storms.

Intensity Measure: an interface variable that is employed between the hazard analysis and the structural analysis.

Landslide: a collapse or substantial movement of a mass of earth or rock from a mountain or cliff.

Material degradation: deterioration of the mechanical properties of the material and/or loss of material mass with time when exposed to the environment.

Observed Engineering Demand Parameter (OEDP): the structural parameter which degradation is to be studied (e.g. deteriorated depth, modulus of elasticity, …)

Unified climatic parameter (UCP): A linear relationship of climatic parameters that are considered to affect the degradation of a building material.

Vandalism: action involving deliberate destruction of or damage to public or private property.

Vulnerability curve: function that provides the distribution of a loss measure given the level of the intensity measure.

1.4 Position in the HYPERION Ecosystem

The HYPERION high-level logical architecture is presented in Figure 3, as defined in Deliverable D2.3 “Architecture Specification” (Krommyda et al. 2020). The dashed red rectangle shows the position of the Multi-Hazard Vulnerability Module (WP5) in the HYPERION Ecosystem. Essentially, MHVMs are created offline via the Structural and Geotechnical Safety Assessment simulator. In more detail, hazard simulators read hazard scenario inputs and feed their output into HRAP. HRAP in turns feeds the hazard input into MHVMs for performing risk and resilience assessment, the results of which are returned back to the middleware for storage.

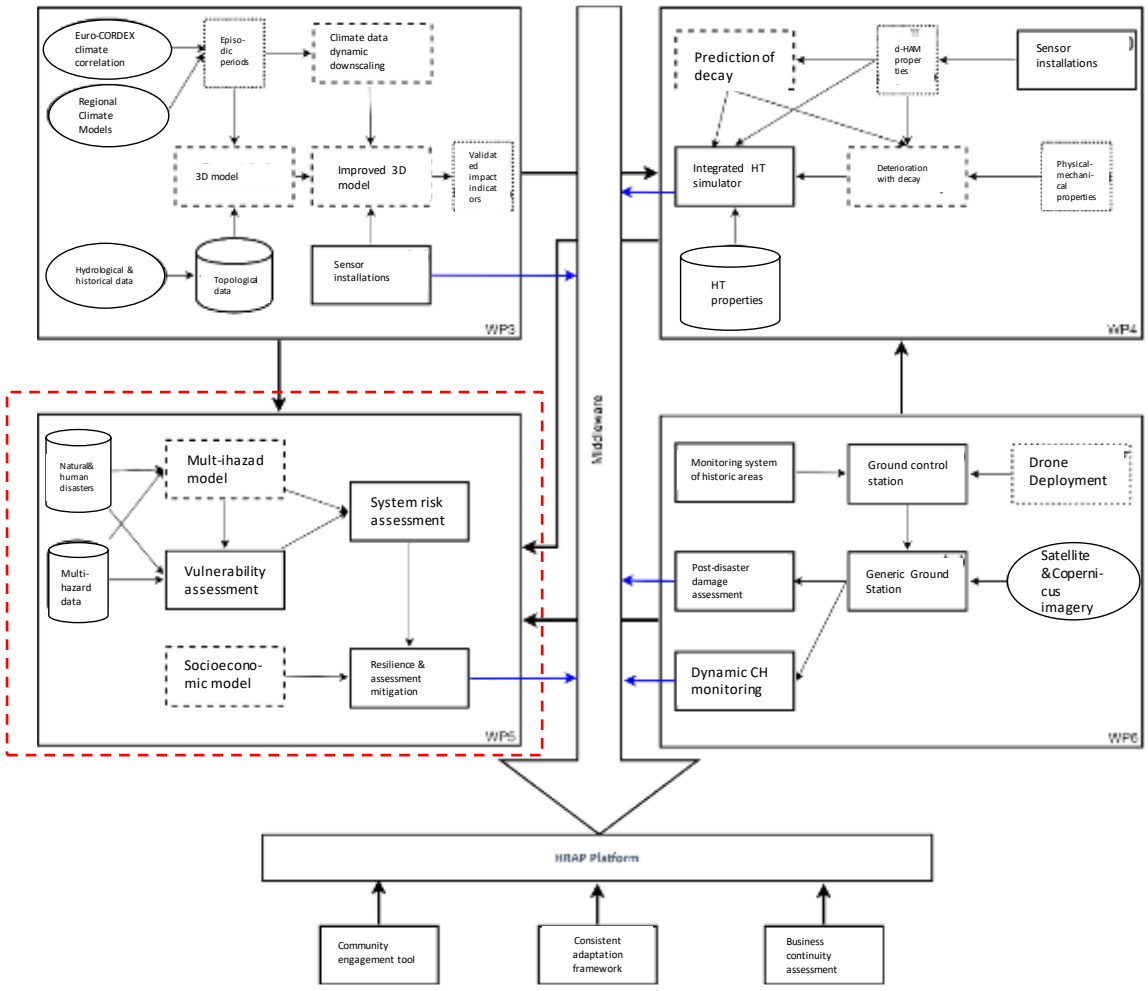

(a) Entire HYPERION Ecosystem

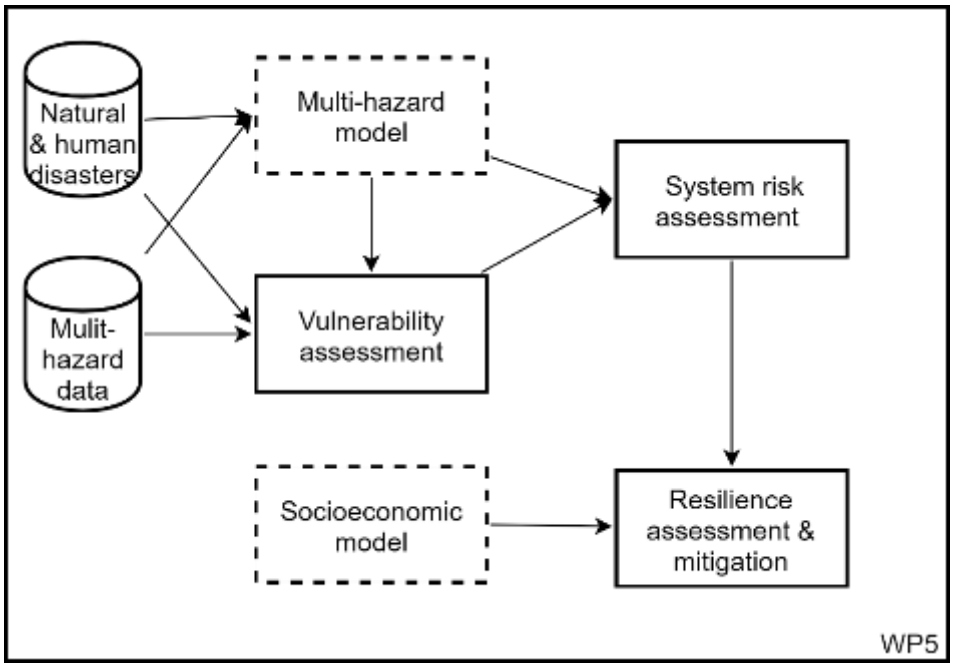

(b) WP5 module: MHVM

Figure 3. Position of the MHVM within the HYPERION Ecosystem, at the heart of "Vulnerability assessment".

2 The methodology

The methodology presented in D6.5 to feed the damage and degradation assessment results into WP5 is developed in two steps.

The first step consists of defining a Unified Climatic Parameter (UPC), which is a linear combination of the climatic parameters that affect a degradation process of a building material.

$$\mathrm{UPC} = \sum_{i=1}^{n} a_i cp_i \quad (1)$$

being a_i the weighting coefficients for a particular building material and for a particular degradation parameter.

In order to obtain a simple representation, easy to compute, the degradation parameter DP (e.g. degradation depth, modulus of elasticity, strength, …) is expressed as:

$$\mathrm{DP} = \beta \mathrm{Tan}[\mathrm{UPC}] \quad (2)$$

Notice that Tan[x] is almost linear for values of x in the interval [-0.5, 0.5], where β is the constant that linearly relates DP with Tan[UPC].

In a second step the observed degradation parameter, named Observed Engineering Degraded Parameter (OEDP) is formulated. OEDP is the structural parameter from which degradation is studied, for example, the OEDP can be the degradation depth or the modulus of elasticity, among others. The measurements of OEDP are analysed in Section 4. Often the OEDP can be measured directly in the cultural heritage buildings. The concept of the OEDP implicitly has more simplified assumptions than the degradation parameter of Eq. 2. Due to this fact, OEDP is formulated substituting β of Eq. 2 for a new constant ξ, and imposing OEDP to be linear with time for constant climatic conditions:

$$\mathrm{OEDP} = t \cdot \xi \mathrm{Tan}[\mathrm{UCP}] \quad (3)$$

Figure 4 shows an example that will be developed later:

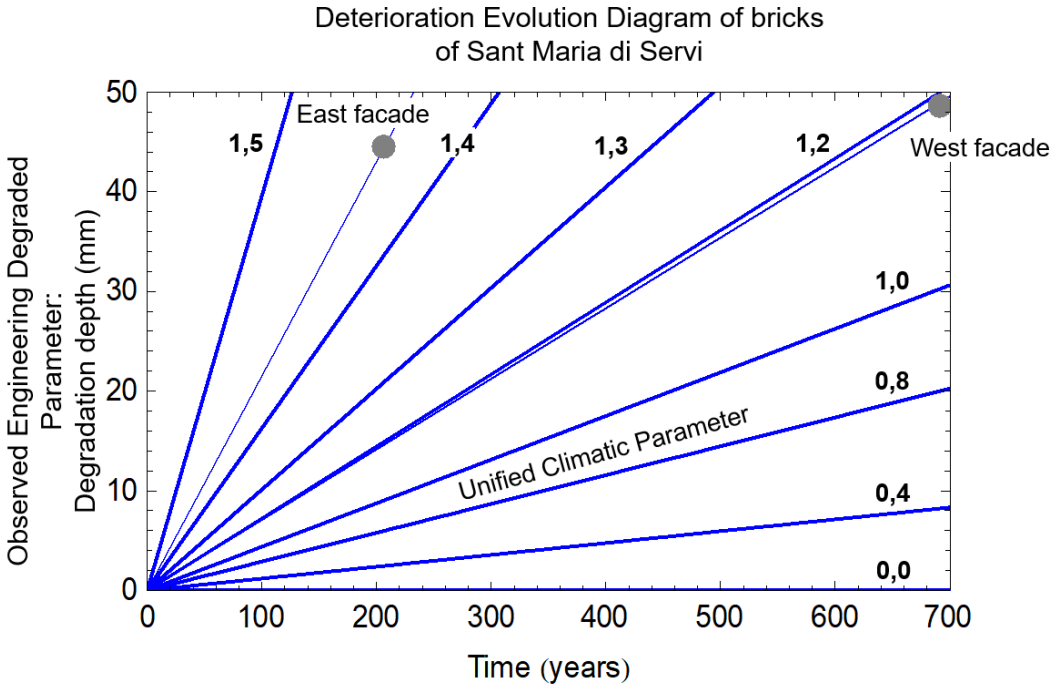

Figure 4. Deterioration Evolution Diagram of the bricks of Santa Maria di Servi (Venice).

In this case the OEDP is the degradation depth of the façade of Santa Maria di Servi (Venice) as a function of time (years) and of the UPC. In this example the UPC is a linear function of freeze-thaw days per year, relative humidity and peak hours of sunshine per day. Due to this last parameter, the two façades of the same building present different level of degradation.

2.1 The hybrid methodology

The hybrid methodology is directly derived from the previous section: the combination of existing models of degradation of materials with the observation of degraded parameters in heritage buildings, see Figure 5.

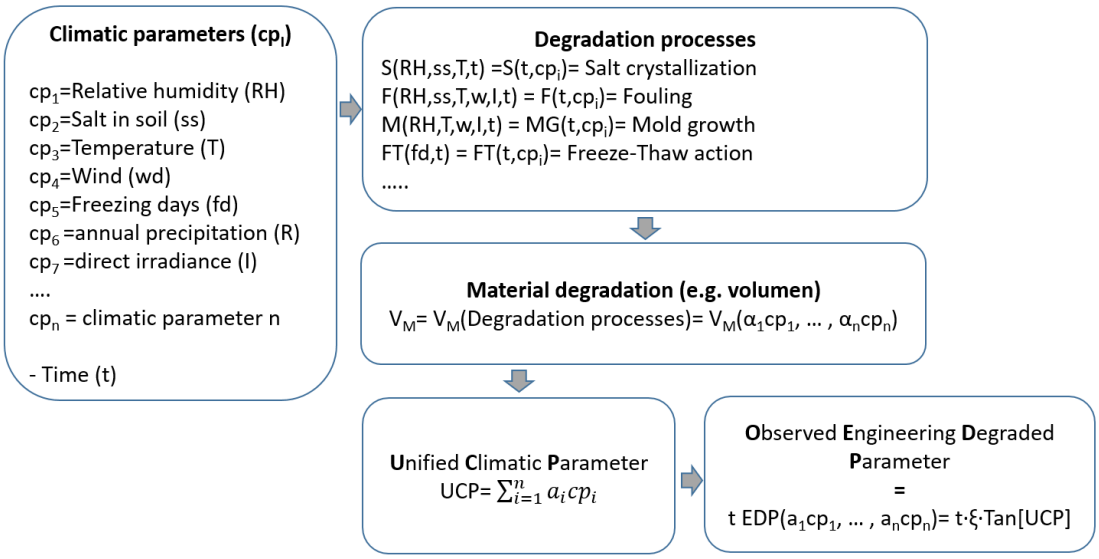

Figure 5. The hybrid methodology

The number of unknowns in Equations 1 and 3 is n+1, being n the number of climatic parameters considered (cp_i). Note that, ξ is also an unknown. The UCP can be obtained from literature or from laboratory data. For the calculation of ξ, the observation of the degraded heritage building is needed.

2.2 The empirical methodology

The proposed methodology, as a whole, is a system n+1 non-linear of equations, which can be solved without considering laboratory data if sufficient information from degraded heritage buildings is available. See Figure 6.

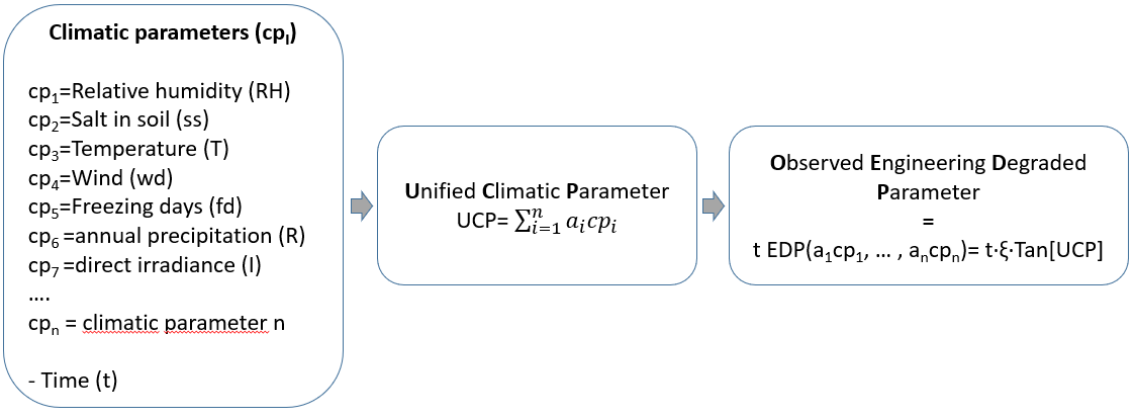

Figure 6. Flow chart corresponding to the empirical method

3 Observation: literature and laboratory

Several studies are available in the literature that relate climatic parameters with material degradation. In particular, for bricks (Coletti *et al.*, 2016), (Yue *et al.*, 2022), some degradation processes has been studied such as: freeze-thaw action for different relative humidity, or salt-crystallization. Figure 7a shows an example of mass loss rate as a function of the number of freeze-thaw cycles and the relative humidity, (Yue *et al.*, 2022). Figure 7b shows an example of mass loss rate for salt-crystallization cycles (Coletti *et al.*, 2016).

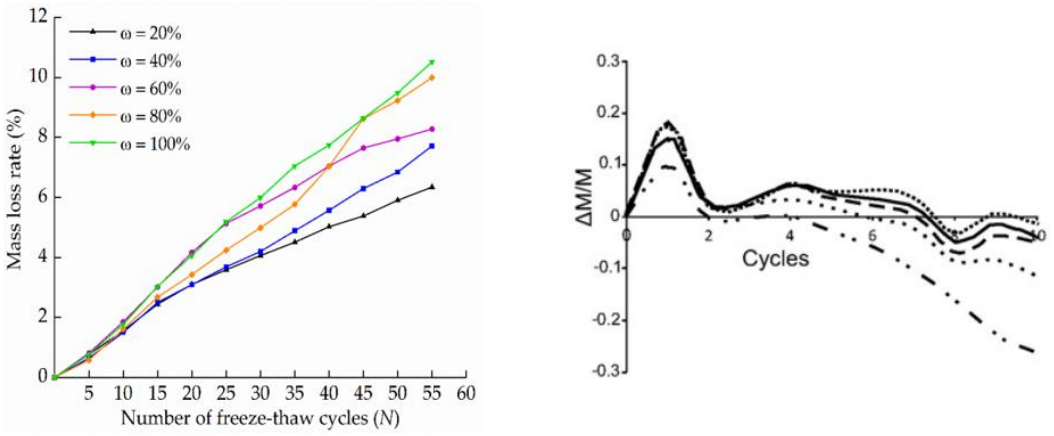

a) Freez-thaw cycles b) Salt crystallization cycles

Figure 7. Mass loss rate for bricks. a) for number of freeze-thaw cycles and relative humidity (Yue *et al.*, 2022), b) for salt-crystallization cycles (Coletti *et al.*, 2016).

In case of calcarenite of Santa Pudia, material widely used in CH of Granada, it has been concluded that the most influential climatic parameter is the number of freeze-thaw cycles, as detailed below.

4 Degradation Observation: field measurements

The two main sources for the analysis of the degradation processes are laboratory data (either made ad hoc or taken from the literature, section 3), and on-site measurement of degraded parameters of heritage buildings. Both sources of information are complementary.

As previously pointed out in Section 2.2, it is important to note that regardless of the method implemented (hybrid or experimental), field measurements cannot be dispensed with, since these measurements allow the laboratory results to be scaled (through the variable ξ), see Equation 3. Various methods have been used for measurements of the degradation of historic buildings, including photogrammetry and laser scanning.

4.1 Tier 1 of Granada. The case of the Monastery of San Jerónimo

Laser scanning (see Figure 8) and photogrammetry have been done in the Monastery of San Jerónimo.

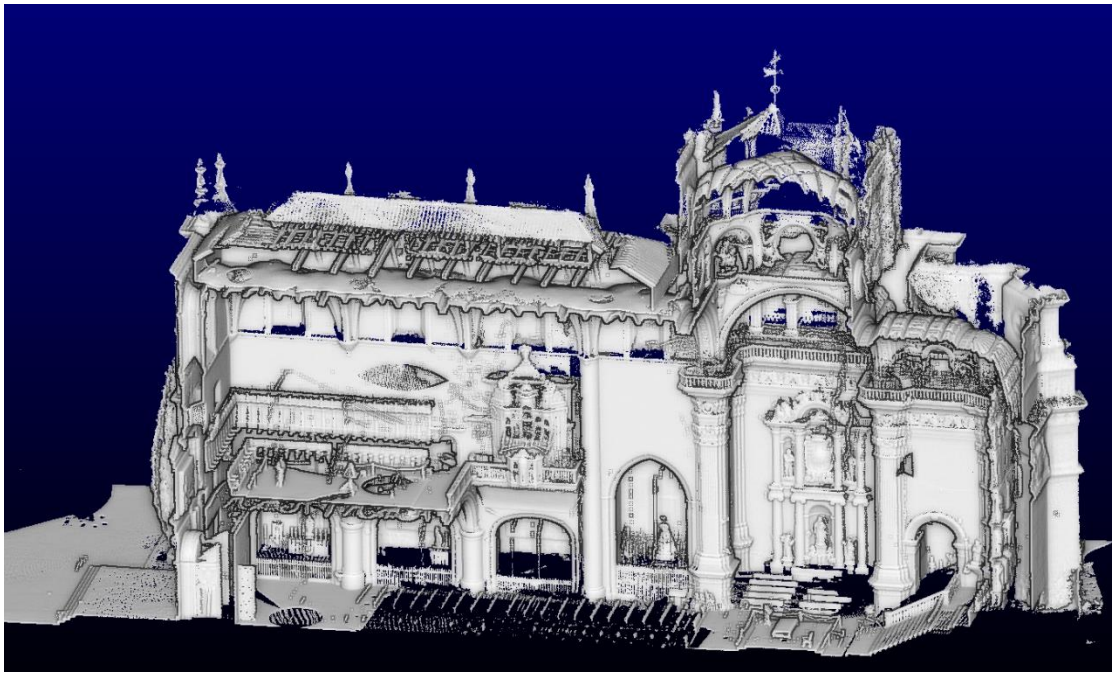

Figure 8. Scan of the interior of the central nave of the Monastery.

Based on photogrammetry, a degradation pattern of the calcarenite in different parts of the Monastery was studied as described in (Jalón *et al.*, 2020). Figure 9 shows some of the locations where the photogrammetric study was done. Figure 10 shows the degradation patterns, average value and different percentiles.

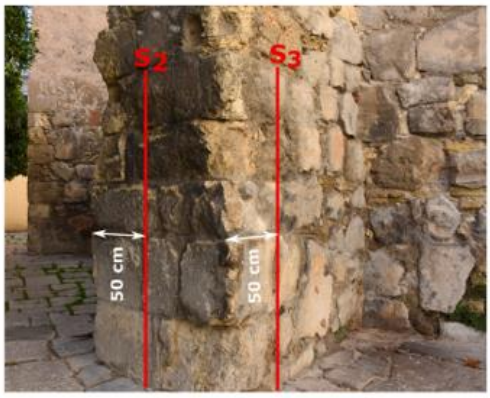

(a)

(b)

Figure 9. Location of the degradation profiles in the building: (a) buttress (section S1 located on the hidden side in the picture), (b) main façade.

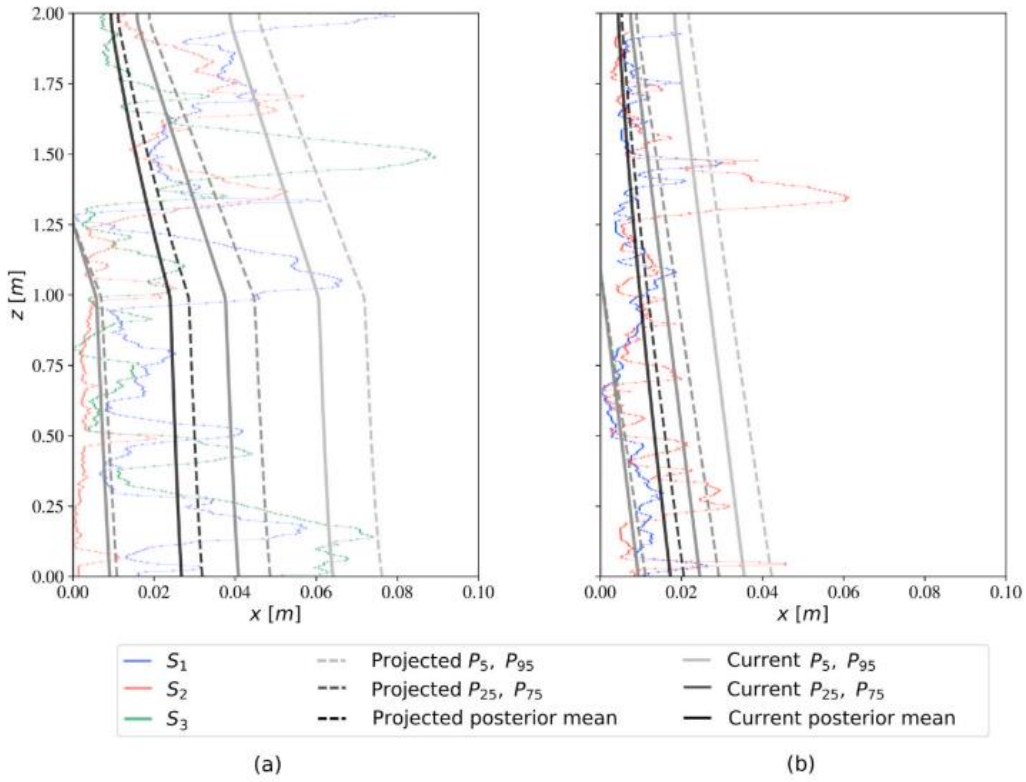

Figure 10. Current and prognosticated posterior mean degradation and confidence intervals (P5, P25, P75, P95) against the experimental degradation data (S1, S2, S3) for (a) the buttress, and (b) the main façade of Monastery of San Jerónimo.

In case of the study of the degradation depth, Figure 10 defines the OEDP to use in Equation 3.

4.2 Tier 2 of Granada. Puerta Elvira and the Mill of the Marquis

Two heritage buildings are considered as study cases for tier 2: the Mill of the Marquis and Puerta Elvira.

The old part of the Mill of the Marquis is made of calcarenite, so the pattern deduce for Tier 1 (San Jerónimo Monastery) is applied to study this CH asset.

Puerta Elvira (PE, Bab Ilvira, see Figure 11) is a fortress gate originally constructed with rammed earth. It was the main access to Granada during the Islamic period and it is one of the oldest gates. PE was built in the 11th century has undergone several transformations being the most significant the one carried out by Yusuf the first in the 14th century. In 1612 the esplanade preceding the gate was levelled and houses attached to the wall were built, which have remained almost unchanged to this day (see Figure 11a). At the present time, the monument of PE is formed by the exterior arch (formed by sandstone voussoirs and preserved from the 14th century), two rammed earth towers that flanked the arch (Figure 11c and d) and the abutment north side of the monument formed by three niches defined by high brick arches that support a walkway (Almagro, Orihuela and Vílchez, 1992), see Figure 11e.

Throughout the 20th century it has undergone several restoration and consolidation works. In 1902 the jambs of the arch were reinforced with calcarenite from Santa Pudia (Almagro, Orihuela and Vílchez, 1992) (Figure 11f). Several repairs have been carried out on the front façade, ranging from simple mortar plaster to more drastic interventions consisting on the inlay of handmade brick pieces to fill gaps produced by the loss of original rammed earth, as in 1957 (Almagro, Orihuela and Vílchez, 1992; A. Almagro and A. Orihuela, 2014) (see Figure 11b).

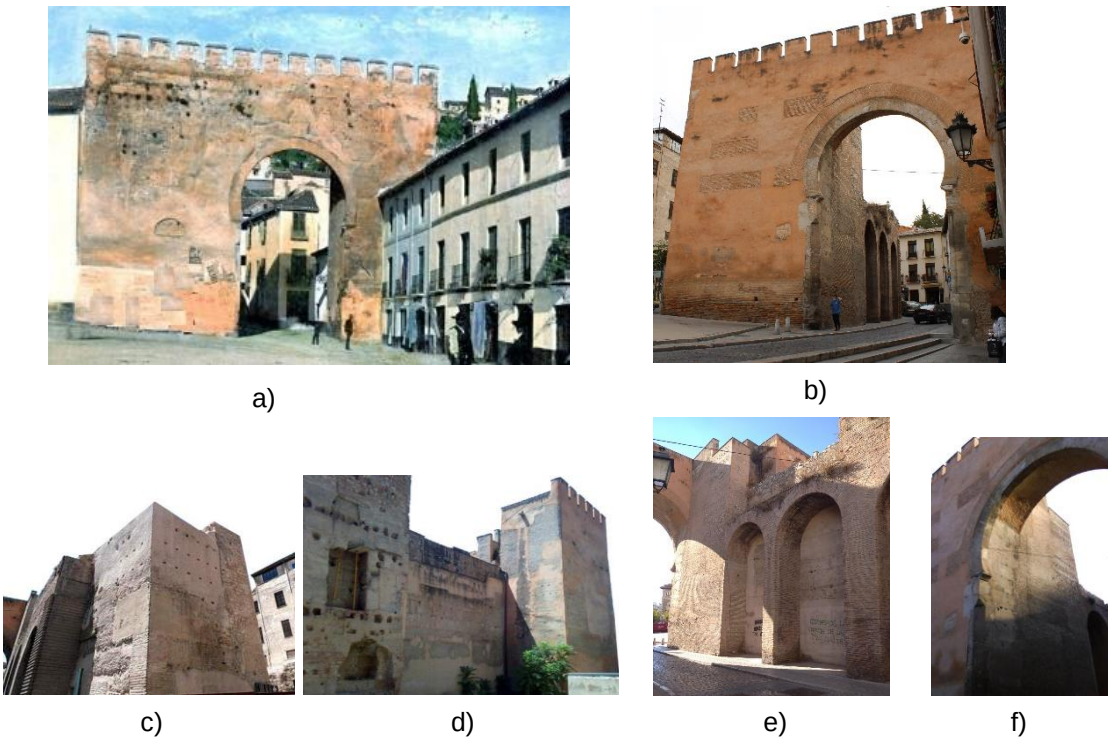

Figure 11. Puerta Elvira, Granada (Spain). a) at early 20th century adapted from (*https://almunecarh.wordpress.com/2013/11/06/granada-ziri-1-puerta-elvira/*, no date); b) to f) at the present time, adapted from (Melchor, 2021).

Because Puerta Elvira was undergone an important restoration with bricks in the lower part of the front façade (the part of rammed earth of the monument more affected by degradation factors), the degradation pattern of rammed earth has been obtained from the Zirid Wall, which were built during the same period.

The Zirid wall is part of the Albaicín wall. It is located in the highest area of the neighborhood of Albaicín (Granada, Spain). The Zirid wall, dated from the 11th century, is one of the oldest monuments in the city. As can be seen in Figure 12, the Zirid wall has hardly undergone any restorations in some of its stretches. In one of such stretches, the pattern of recession of the rammed earth wall has been obtained by using digital photogrammetry data.

Figure 13 shows the location of the selected portion of original wall and the process of taking photos.

Figure 12. Zirid wall. Photogrammetry of the site.

The digital photogrammetry is used as non-destructive technique for mapping degradation data. Several high-resolution images are taken using a digital still camera (Nikon D7200, 18 mm focal length), a tripod and a remote shutter connected to the camera's wifi to take photos without disturbing the camera. Then, the digital images are processed out of digital images and 3D spatial data are generated, denoted as photogrammetric point cloud (PPC). The degradation sections are extracted from the PPC using the open source software CloudCompare (Girardeau-Montaut, 2016), a 3D point cloud and mesh processing software. Then the data is exported in a suitable format to be read.

The model of the wall was made by overlapping several images (see vertical lines in Figure 13) after manually prepare each of them. In this case, 21 sections of reference separated at 0.5 m are considered along the stretch studied of the Zirid Wall. Figure 12 shows the high level of deterioration of this portion of the Zirid wall. As can be seeing, along the 2 meters analysed, deep cavities exist. The wall is affected by similar degradation at both sides. In this work, the inner side of the wall is studied (i.e. the Granada city´s side).

To obtain the degradation pattern of the rammed earth six sections (S1 to S6) of the 21 ones indicated in Figure 13 are considered. Because the most significant degradation agents (such as: water run-off, moisture, freeze thaw cycles, …) act at the lower part of the wall, the selected sections are the ones at which the rammed earth is located from the ground level up as can be seen in Figure 13.

Degraded sections S1 to S6 are represented in Figure 14. As can be seen, the degradation effect affects up to 1.4 meters height and 0.6 m depth. Once the

sections are geometrically defined, the degradation pattern is obtained based on lineal regression. Given the shapes of the degraded sections, a rectangular candidate degradation profile (see Figure 14b) is considered, which represents reasonably well the experimental data. In Figure 14b mean and 5 th, 25 th, 75th and 95th percentiles are indicated. As can be seen in Figure 14b, the mean values of the degraded height and depth are 0.32 and 1.14 m, respectively.

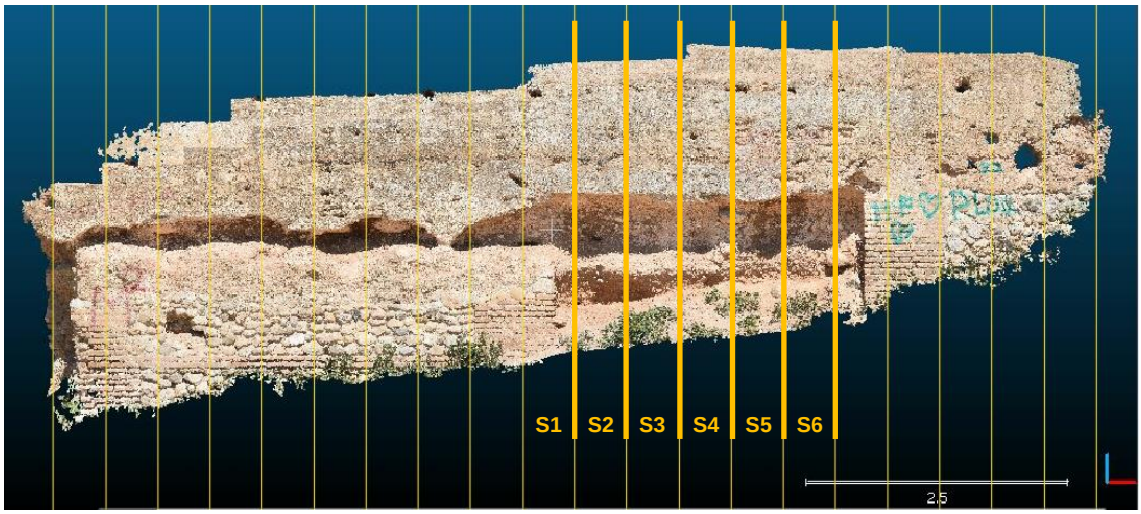

Figure 13. Photogrametric reconstruction of the stretch study of the Zirid Wall. Location of reference sections. CloudCompare.

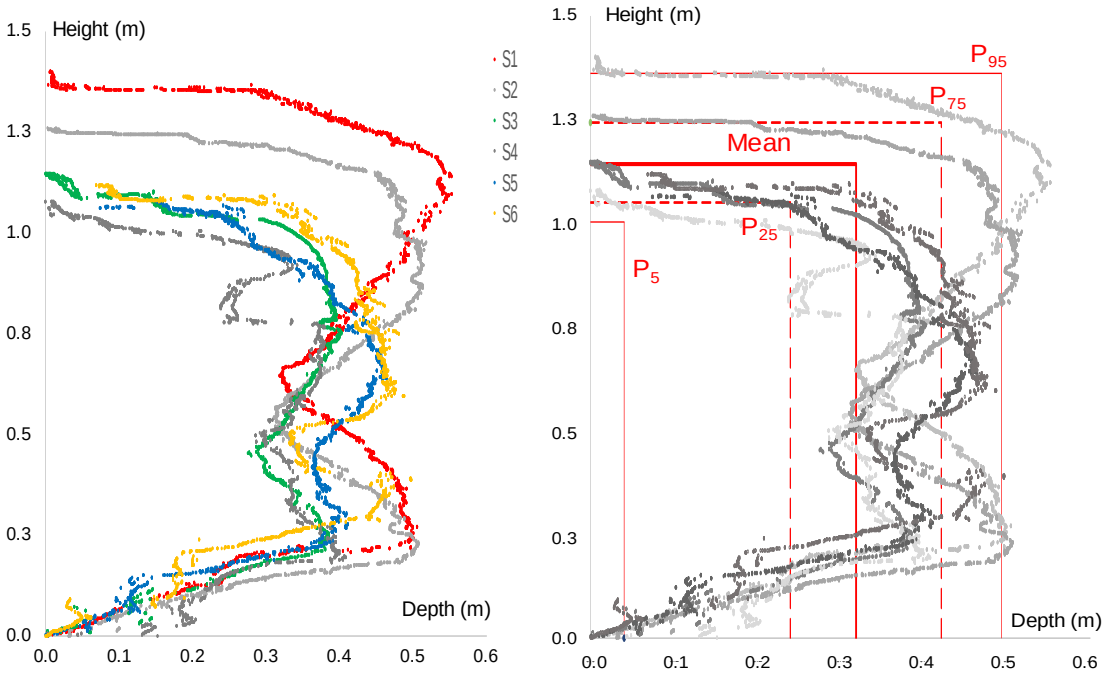

Figure 14. Degradation pattern of rammed earth. a) Sections studied (see Figure 6). b) Rectangular adjusted degraded profiles of rammed earth from linear regression.

4.3 Tier 2 of Venice. Santa Maria di Servi

Deterioration of the West and East façades of Santa Maria di Servi are studied using photogrammetry.

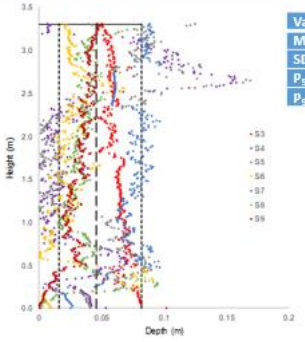

Values in meters	Front	Back
Mean degradation	0.046	0.201
SD	0.027	0.137
P_5	0.016	0.016
P_{95}	0.082	0.375

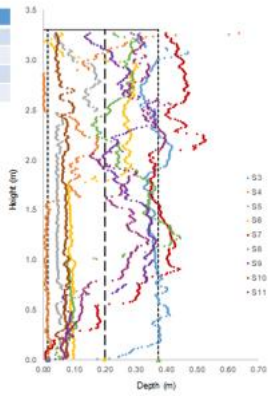

5 Linking damage with CC

5.1 Granada case

The particularity of the orography of the province of Granada is ideal to apply the methodology presented in D6.5 in a fully empirical version (Section 2.2). Granada province presents several climatic environmental conditions at short distances apart, from 0 to 3700 meters above sea level in less than 50 kilometers.

In order to consider the influence of the different climate conditions on the calcarenite stone, three CH buildings made with calcarenite from the same quarry, with different environmental conditions have been located and studied.

The initial study is based on photogrammetry. Figure 15 shows the three locations, the name of the buildings, and the main environmental characteristics of these places. Figure 16 shows the two other buildings studied besides San Jerónimo.

HISTORICAL BUILDING	CONSTRUCTION YEAR	LOCATION	Temperature (Cº)			Humidity (%)	Rain (mm)
			Mean	Max	Min		
San Jeronimo monastery	1590	Granada (urban area)	15,3	32,8	1,1	57,4	536
Del Carmen church	1589	Alhama de Granada	13,3	29,0	10,3	65,9	704
De Nuestra Señora del Rosario church	1573/1778	Velez de Benaudalla	17,3	28,6	13,4	67,3	416

Figure 15. Point Location of the three locations and CH buildings. San Jerónimo in Granada, del Carmen Church in Alhama de Granada, and Nuestra Señora del Rosario Church in Vélez de Benaudalla.

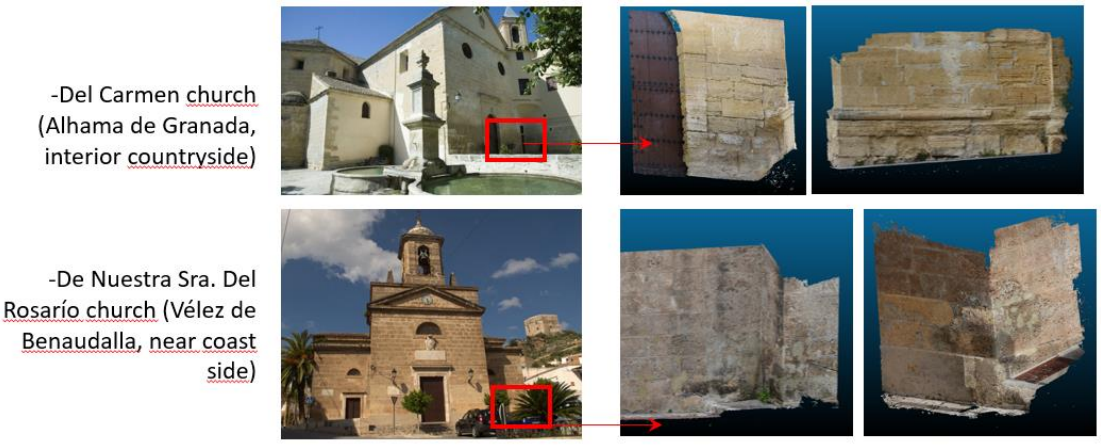

Figure 16. Del Carmen Church in Alhama de Granada, and Nuestra Señora del Rosario Church in Vélez de Benaudalla.

Figure 17 shows the measured cross-sections at Del Carmen Church in Alhama de Granada and the current state of the two facades photographed. The eight cross-sections studied together with their means and standard deviations values are also shown in Figure 17.

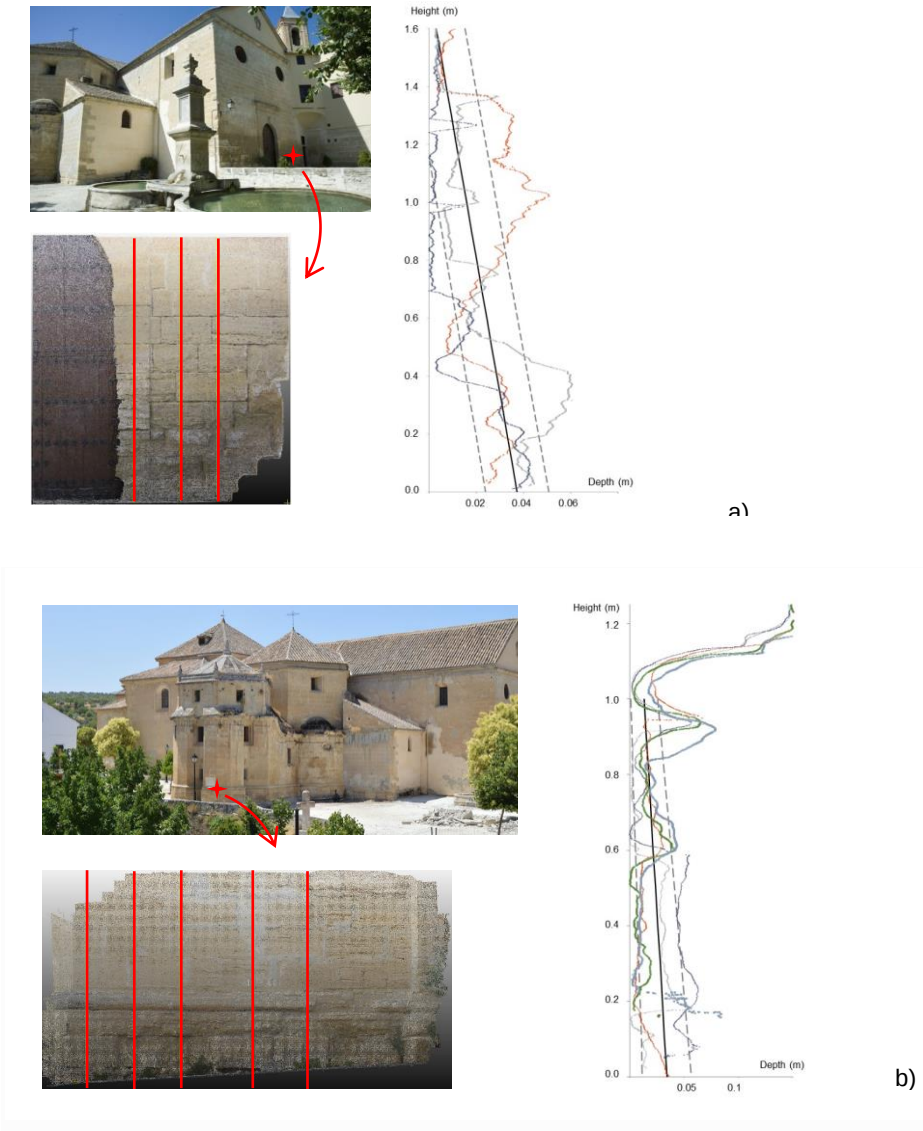

Figure 17. Recession patterns of Alhama de Granada. a) Main façade (NW orientation). b) Lateral façade (NE orientation)

Table 1 summarizes the main parameters measured in the three monuments. Triangular degradation patterns have been considered, as suggested in (Jalón et al., 2020) for calcarenite in Granada. The mean degraded area and the standard deviation of the adjusted degradation patterns are shown in the last two columns of Table 1. It can be observed that degradation is less important in Nuestra Señora del Rosario in Vélez de Benaudalla, a location near the coast. The higher level of degradation appears in the buttresses behind apse of San Jerónimo monastery. Figures 9 and 18.

Table 1. Average area affected by degradation.

Location Heritage building	Year of construction	masl	Location	Affected height (m)	Average degraded area (m^2)	Standard deviation (m^2)
Alhama de Granada	1589	895	Main façade (NW)	1.60	0.0323	0.012
			Lateral façade (NE)	1.00	0.0238	0.006
Vélez de Benaudalla	1778	173	Main façade (SE)	2.75	0.0003	0.002
			Corner (S)	2.50	0.0013	0.002
Granada	1519	689	Main façade (NW)	2.00	0.0084	0.0001
			buttres (SE)	2.37	0.0500	0.0079

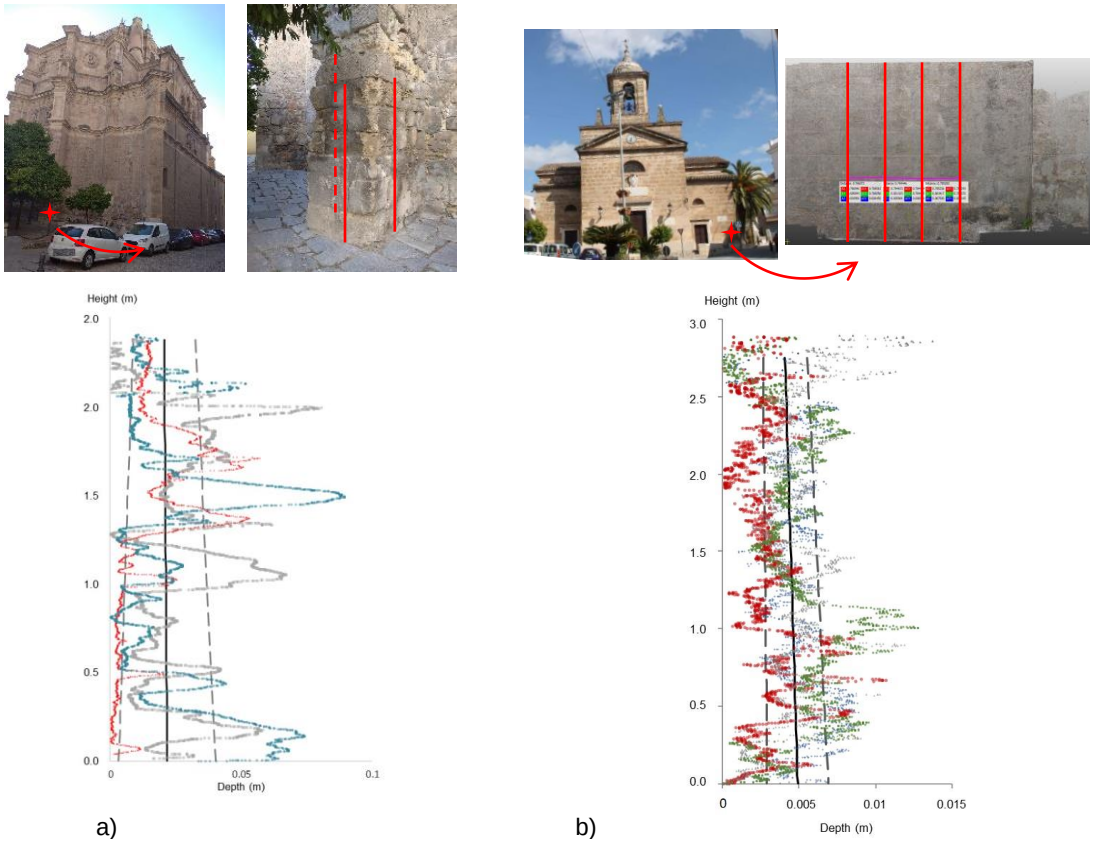

Figure 18. Recession patterns of a) Butress of San Jerónimo in Granada, b) Main façade of Nuestra Señora del Rosario in Vélez de Benaudalla.

Aging of heritage buildings is mainly manifested at the exterior facades, which means an aesthetical deterioration and a decrease in its structural capacity. Evidence shows

that in most of the cases the parts of the buildings closer to the ground are the more affected ones by deterioration.

Materials present different types of environmental vulnerabilities. It is known that the content of water is a key factor in the phenomena of stone deterioration (Lerma, Cabrelles and Portalés, 2011; Ghobadi and Torabi-Kaveh, 2014). Water affects significantly the material behaviour and may cause structural damage. Indeed, deterioration due to water (moisture and/or rain) can be due to several causes such as chemical dissolution (Maravelaki *et al.*, 1992) or mechanical action associated with the changes of volume when temperature drops below zero degrees (freezing–thawing).

Due to the importance of SPC in the cultural heritage of Granada, this stone has been widely studied. A detailed work about the petrographic and physical characteristics of SPC was carried out in (Molina Piernas, 2015), its durability and the effectiveness of treatments in order to enhance it was studied in (Cultrone, Sebastia and Ortega Huertas, 2007; Luque *et al.*, 2008; Molina *et al.*, 2011, 2013; Vázquez *et al.*, 2013) and the influence of vehicle exhaust gases in the degradation of this limestone was studied in (Rodriguez-navarro and Sebastian, 1996). Recently, the main mechanical properties (compressive strength, elastic modulus and Poisson's ratio), the effect of high temperatures in the compressive strength and the creep behavior of SPC has been studied through their corresponding tests (Gil-Martín, Fernández-Ruíz and Hernández-Montes, no date).

SPC has a value of open porosity of 32,8 $\pm$ 2,3% (Molina *et al.*, 2013). It is known that pore system of sedimentary rocks is a key factor in the durability of building materials (Molina *et al.*, 2011), being limestone very sensitive to dissolution and freeze–thaw weathering (Ghobadi and Torabi-Kaveh, 2014).

Table 1 shows that the mean deteriorated area in Del Carmen Church in Alhama is 0.028 m^2, which leads to an average loss of 64.87 mm^2/year. In the case of the San Jerónimo Monastery, the average loss is 58.17 mm^2/year, while in the Rosario church (near the coast) it is 0.32 mm^2/year.

In light of Table 1, it can be concluded that the number of freeze/thaw days is more relevant in the degradation of the SP calcarenite than the annual precipitation itself. The foregoing is compatible with the fact that, due to the high porosity of the SP calcarenite, the dew water, which penetrates the rock every day, could be a factor that favors the degradation of this stone when it is subjected to daily freeze/thaw cycles. Nevertheless, both climatic parameters have been considered, expanding Equation 3 to a system of 3 equations with three unknowns (ξ, a_1 and a_2):

$$\begin{aligned} 0.02805 &= 432 \cdot \xi \,\mathrm{Tan}[49.77a_1 + 791.08a_2] \\ 0.0008 &= 243 \cdot \xi \,\mathrm{Tan}[0.36a_1 + 405.39a_2] \\ 0.0292 &= 502 \cdot \xi \,\mathrm{Tan}[49.11a_1 + 196.64a_2] \end{aligned} \quad (4)$$

Resulting in ξ=0.0001022, a_1=0.01025 and a_2=0.00007030. The obtained deterioration function has been represented in Figure 19 for different values of the UCP.

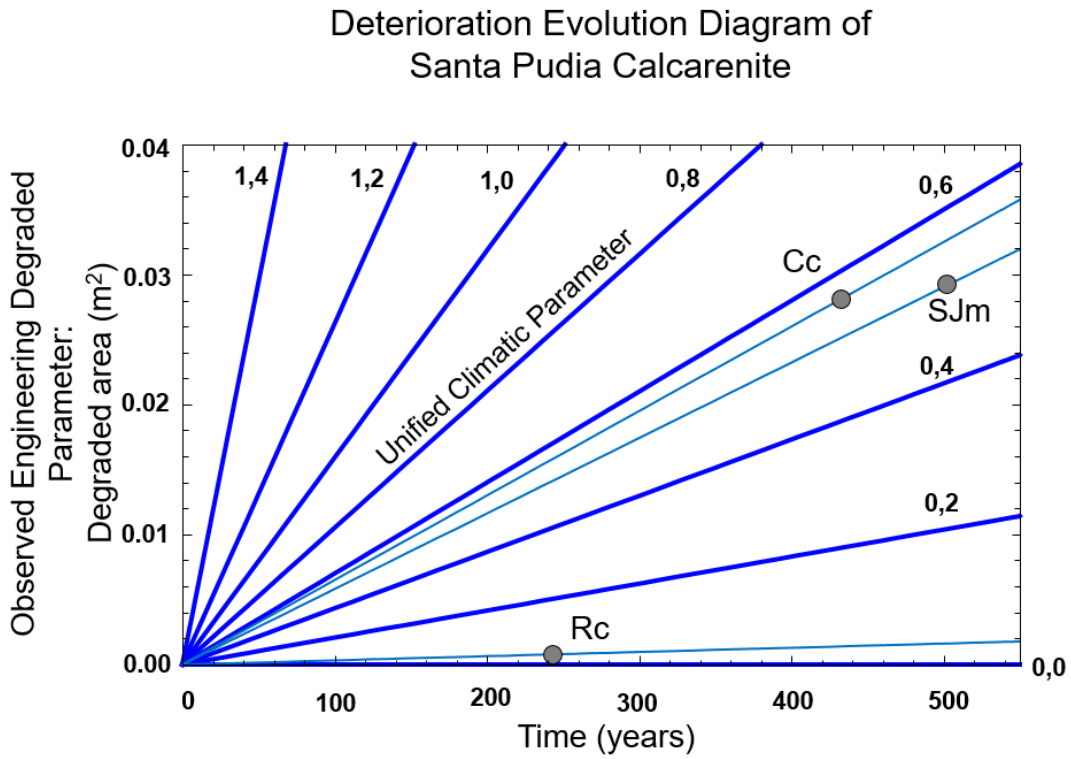

Figure 19. Deterioration function depending on the age and the unified climatic parameter. Legend: Cc= Del Carmen church in Alhama de Granada, Rc= Rosario church in Vélez de Benaudalla, SJm= San Jerónimo monastery in Granada.

5.2 Santa Maria di Servi

As previously said, the UCP is a weighted linear combination of the climatic parameters that affect the OEDP considered. For the study of the bricks used in Santa Maria di Servi three climatic parameters have been used: freeze-thaw days per year, relative humidity and peak hours of sunshine per day. These parameters have been chosen because freeze-thaw cycles and salt-crystallization processes are the most degraded phenomena in this type of bricks.

Figure 7, extracted from (Yue *et al.*, 2022), shows the mass loss rate as a function of the number for free-thaw cycles and humidity for a particular brick. These authors tested 50×50×50 mm bricks, so the loss of volume can be expressed as the recession of the surface B1 as:

$$B1 = \frac{50}{6}\frac{\text{mass loss rate}}{100} \quad (5)$$

Figure 7 shows that the behavior present some inconsistencies (e.g. the erratic tendency corresponding to 80% HR). Moreover, the RH is a variable that in ambient conditions, is between 80 and 40%. Due to this behavior, only the values of 80 and

60% of RH for 50 freeze-thaw cycles are considered to calculate the weight of the number of freeze-thaw cycles and relative humidity on the UPC variable:

$$\left.\begin{aligned}\frac{50\cdot 0.92}{600} &= \mathrm{Tan}[50\,a_1 + 0.8\,a_2]\\ \frac{50\cdot 0.80}{600} &= \mathrm{Tan}[50\,a_1 + 0.6\,a_2]\end{aligned}\right\} \rightarrow \begin{aligned} a_1 &= 0.0007344\\ a_2 &= \quad 0.04974\end{aligned} \tag{6}$$

Salt-crystallization cycles is an important factor of deterioration, as shown in (Coletti *et al.*, 2016), from a study on 50×50×50 mm bricks. The peak hours of sunshine per day is a climatic parameter that is capable of distinguishing the influence of deterioration due to salt crystallization in different orientations of a specific site. The east façade has 1.81 peak hours of sunshine per day, while the west façade has 1.49 hours (https://footprinthero.com/peak-sun-hours-calculator). The west façade has been outdoors since 1330 while the east façade since 1815 due to the demolition of the roof of church.

Due to the shape of the degradation in the façades (Figure 20 and 21), a constant degradation thickness along the height of the façade has been considered as OEDP.

Figure 20. Photogrammetric study of the west façade of Santa Maria di Servi, Venice.

In the last twenty years Venice presents a mean relative humidity (RH) of 69.1% and 4 frost days (n_{fd}). Deterioration is formulated following Eq. (3), in which the salt-crystallization effect has been added to annual precipitation and free-thaw cycles per year. Note that when implementing Eq. (3) the number of freeze-thaw cycles is considered to be the number of frost days per year (n_{fdy}). Relative humidity (RH) and the peak sun hours per day (n_{psh}) are the other two climatic parameters studied.

$$\mathrm{OEDP} = t\cdot\xi\,\mathrm{Tan}[a_1 n_{fty} + a_2 \mathrm{RH} + a_3\, n_{psh}] \tag{7}$$

From photogrammetric data, see Figure 20, the west façade has an average recession of 0.049 m, so Eq (3) is particularized as:

$$49 = 692\cdot\xi\,\mathrm{Tan}[0.000734\, n_{fty} + 0.0497\,\mathrm{RH} + a_3 1.49] \tag{8}$$

The deterioration expression has two unknowns: the salt-crystallization weighting coefficient (a_3) and ξ.

The east façade has been altered along its history, being difficult to obtain a total recession rate. Only the upper part of Section 3 (S3), at both sides of the wall, seems trustful, see Figures 20 and 21.

Figure 21. Photogrammetric study of the east façade of Santa Maria di Servi, Venice.

The top part of both sides of Section 3 have been compared to obtain a second equation of the recession, Equation 9. In case of a constant recession, the difference between both sides is 4.375 mm.

$$4.375 = 692\cdot\xi\,\mathrm{Tan}[0.000734\,n_{fty} + 0.0497\,RH + a_3 1.49] - 207\cdot\xi\,\mathrm{Tan}[0.000734\,n_{fty} + 0.0497\,RH + a_3 1.81] \quad (9)$$

Solving Equations 8 and 9 for n_{fty}=4 and RH=0.691, results in ξ=0.0277 and a_3=0.765.

Obtaining the UPC and the recession values:

$$OEPD = 0.0281\cdot t\cdot\mathrm{Tan}[UPC]$$
$$UPC = 0.000734 n_{fty} + 0.0494 RH + 0.7756\,n_{psh} \quad (10)$$

Equation 10 is plotted in Figure 22.

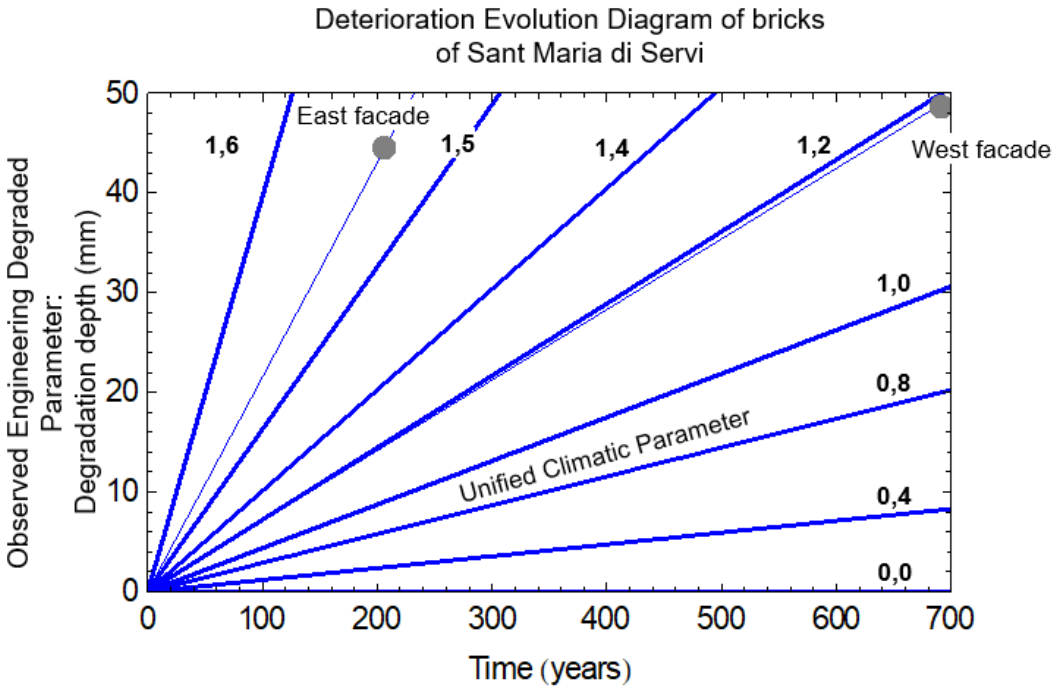

Figure 22. Deterioration Evolution Diagram of the bricks of Santa Maria di Servi, Venice.

6 Risk analysis

6.1 Numerical models

Numerical analysis is used widespread for solving dynamic problems. If the level of seismic activity is low enough, the damage caused to the structure due to seismic loading can be assumed to be quite small and distributed. In such situation a continuous approach can be done for the structure and simple finite element models can be used for the analysis.

Both the Monastery of San Jerónimo and Puerta Elvira have been analyzed numerically to obtain their fragility curves. The models were restrained at ground level and, after been subjected to the action of its own weight, accelerations in two perpendicular directions induced by the accelerograms designed for Granada were imposed at the nodes of the ground level of the FE model. Ten sets of artificial accelerograms **a**(t) were selected for the numerical analyses by combining their N-S and W-E components. See Section 6.2 for more information about hazard analysis, disaggregation and record selection.

Puerta Elvira (PE has been modelled using 3D solid finite elements defined by eight nodes having three degrees of freedom at each node: translations in the nodal x, y, and z directions. As can be seen in Figure 23, the model of PE has three materials: rammed earth, Santa Pudia calcarenite (this stone was one of the most commonly

used building materials in the construction of historical buildings in the city of Granada) and bricks.

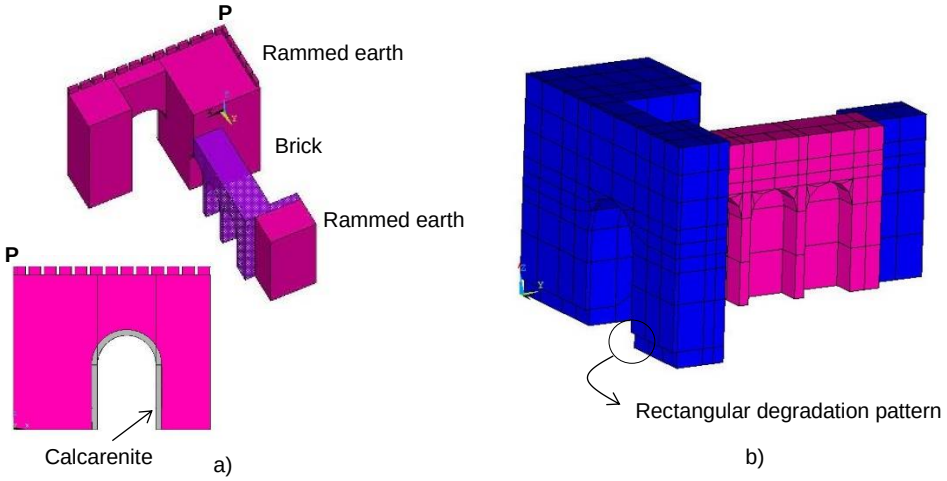

Figure 23. FE model of Puerta Elvira.

Regarding the Monastery of San Jerónimo, the FE model was built using shell elements. The material of the monastery was calcarenite of Santa Pudia, concrete in the upper part of the tower (dark gray in Figure 24) and brick fabric for the domes (in blue in Figure 24). The σ-ε curve of the SPC material was experimentally obtained from monotonic compression tests of several specimens (Figure 25).

The Unconfined Compressive Strength (UCS) of the rammed earth was experimentally obtained from specimens prepared in laboratory. The earth material was hand-mixed with the optimum moisture content (8% by mass). A cylindrical mold (15 cm diameter, 30 cm height) was used to prepare the samples. Consequently, the resulting RE samples had an aspect ratio of 2 (it is important to avoid smaller aspect ratios according to (Aubert *et al.*, 2013)). The moist soil was poured into the mold and compacted in 6 layers with 2 kg of material for each one. Each layer received the Proctor Energy (E = 0.583 J/cm^3), which was measured with a manual rammer. The objective of this manufacturing strategy is to obtain a RE sample as similar as possible to in situ material. After the compaction process, the RE samples were removed from the molds and left drying for 4 months in normal atmosphere. They were considered "air-dry" when moisture content remained constant, which occurred approximately at the 25th day. Finally, the bottom and top surfaces of the RE samples were capped with a mortar in order to provide a flat smooth surface. The average σ-ε compression curve is represented in Figure 25.

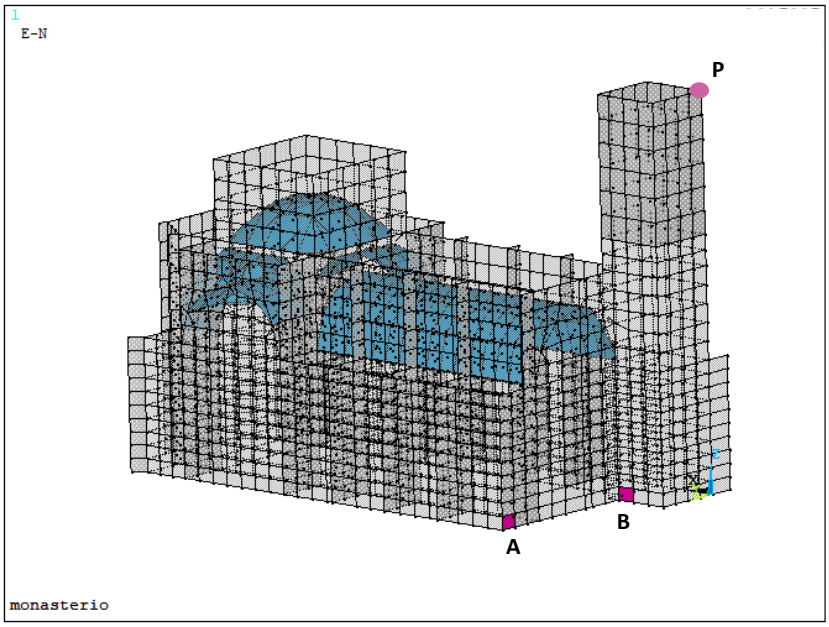

Figure 24. FE model of San Jerónimo

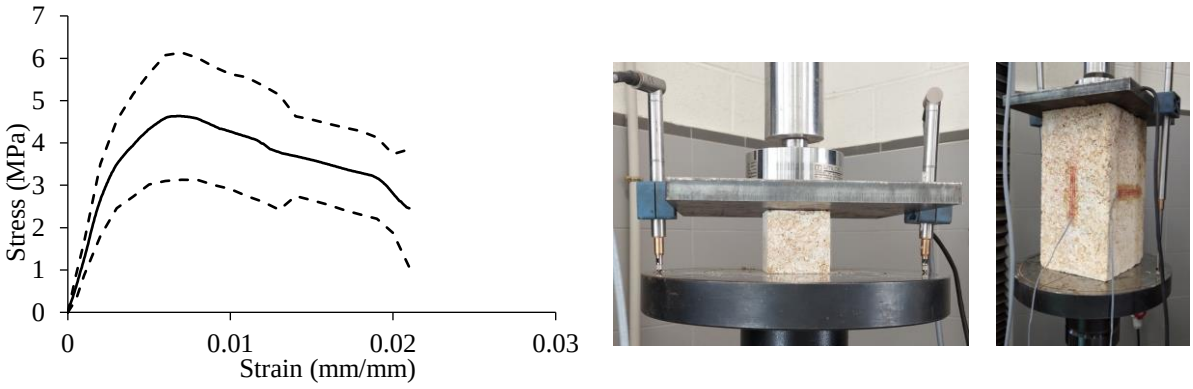

Figure 25. (a) Experimental results of compression tests of SPC, (b) uniaxial compression test setup, (c) test setup for determining the Elastic Modulus.

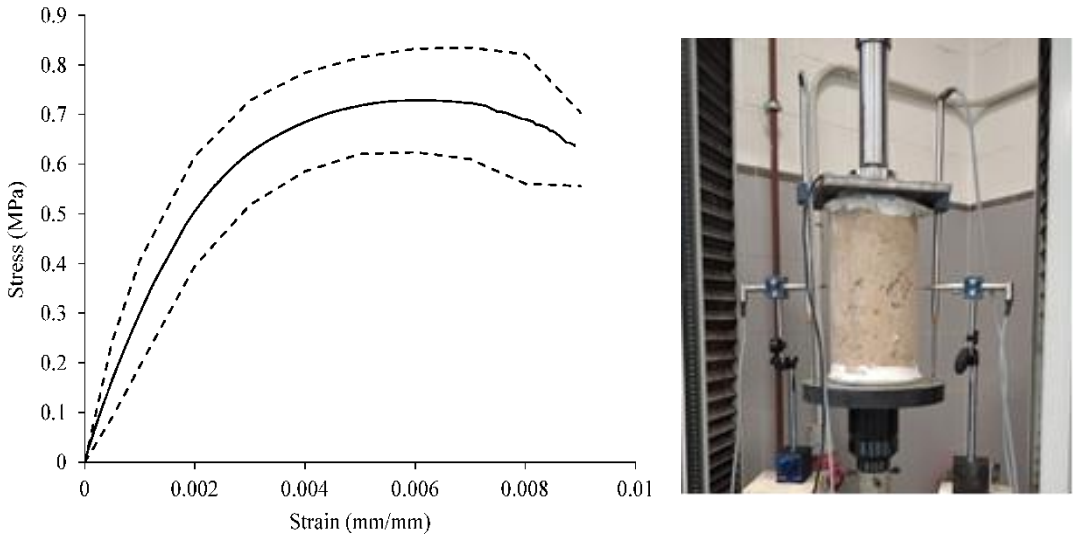

Figure 26. Average stress-strain curves of all the RE samples tested (black curves). Dashed black curves correspond to the standard deviation of compressive stress

In the numerical analysis, rammed earth has been modelled as a very poor concrete having cracking and crushing capacities that are defined by a failure surface. This surface defines cracking or crushing depending on whether the principal stress is tensile or compressive, respectively. In compression, crushing corresponds to the complete deterioration of the structural integrity of the material. In tension, the behaviour is linear elastic until failure. The failure surface does not consider strain softening neither in compression nor in tension and therefore, when stresses in one direction reach the failure surface it drops to zero suddenly (K.J. William and E.D. Warnke, 1975). The behavior of rammed earth in compression considered in the numerical model corresponds to the average stress-strain curve represented in Fig. 25. The mean Poisson´s ratio experimentally obtained is also considered in the numerical model (i.e. $\nu = 0.21$).

In order to improve the convergence in the finite element analysis, a meshing with cubic and rectangular elements respectively have been used.

Both, non-degraded and degraded FE models are analysed. The latter is modeled by eliminating a block of material of the lower part of the front façade, which is the most affected by degradation (see Figure 27). Dimensions of the degraded area are the one indicated in Fig. 10 (current posterior mean) for San Jerónimo and the mean adjusted profile in Fig. 14 for the rammed earth (i.e. 0.32 m depth and 1.14 m height, for Puerta Elvira.

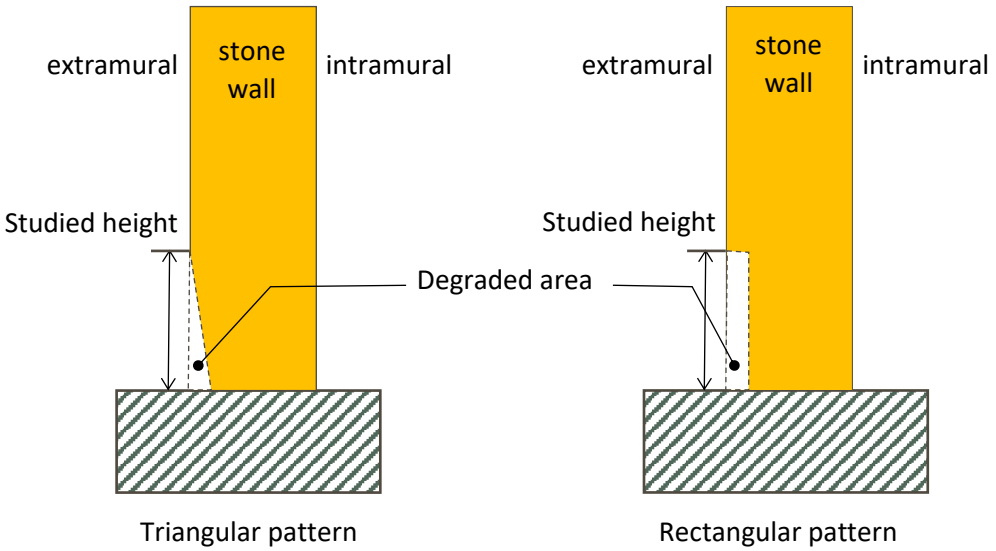

Figure 27. Degradation patterns types: triangular for SPC and rectangular for rammed earth.

Brick masonry wall is modelled with E=900 MPa with a compressive strength of 5 MPa. A tensile strength equal to 0.2 MPa was considered for all the materials to allow convergence. Densities are 1750, 2000 and 1900 kg/m3 for calcarenite, rammed earth and brick wall respectively. The failure of the three materials is defined by the multilinear isotropic material which uses von Mises failure criterion, along with the Willam and Warnke model (K.J. William and E.D. Warnke, 1975).

Given the lack of information, the Rayleigh damping constants (mass-proportional and stiffness-proportional, respectively) were obtained from the two first undamped natural frequencies considering a damping ratio of 5% (Aschheim, Hernández-Montes and Vamvatsikos, 2019). Neither creep nor stiffening degradation have been considered in the numerical model.

6.2 Accelerograms for the site of Granada

Accelerograms have been obtained from a Probabilistic seismic hazard analysis (PSHA) performed for Granada. The SHARE area Source model was adopted considering all the sources within 200 km from the sites (Giardini, Woessner and Danciu, 2013). To consider the type of soil in the hazard analysis a value of Vs30=400 m/s has been assigned. Hazard and record selection computations were based on BA08 GMPE model (Boore and Atkinson, 2008) and both hazard and disaggregation analyses were performed with OpenQuake (version 3.10.1) (Monelli et al., 2012).

The hazard analysis is performed for AvgSA (defined as the geometric mean of spectral accelerations) in the period range of [0.2, 2.0]s with an increment of 0.1s. The hazard curve is shown in Figure 28.

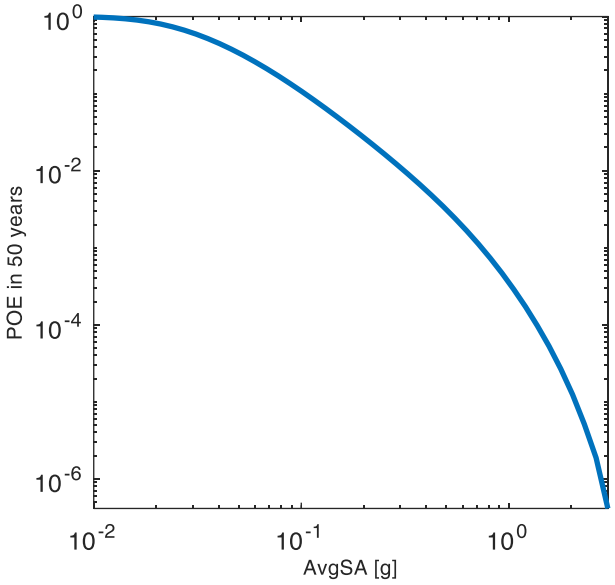

Figure 28. Hazard curves at the selected site in terms of AvgSA. Note that AvgSA corresponds with the geometric mean spectral acceleration in the range [0.2, 2.0]s with an increment of 0.1s.

The IM values correspond with 70.0, 50.0, 30.0, 10.0, 5.0, 2.0, 1.5, 1.0 and 0.6 % of exceedance in 50 years are shown in Table 2. As can be seen in Table 2, the IM value for 475 years in terms of AvgSA is 0.104g. In this table the values of mean magnitude ($\overline{M}$) and mean distance from rupture ($\overline{R}$) and epsilon (what is epsilon can be seen in (Baker and Cornell, 2005)) are also summarized.

Table 2. IM value, mean magnitude, distance and epsilon. IM is given in [g].

IM Level	% in 50 years	Granada			
		AvgSA [g] (IM value)	$\overline{M}$	$\overline{R}$ [km]	ε
1	70	0.026	5.73	52.3	0.81
2	50	0.037	5.82	45.8	0.88
3	30	0.054	5.92	38.2	0.95
4	10	0.104	6.08	26.4	1.06
5	5	0.148	6.17	20.9	1.10
6	2	0.230	6.29	15.7	1.16
7	1.5	0.262	6.33	14.4	1.19
8	1	0.313	6.38	13.0	1.23
9	0.6	0.387	6.44	11.7	1.30
10	0.2	0.587	6.57	10.0	1.50

Disaggregation analysis (Bazzurro and Cornell, 1999) was conducted for each IM level. Figure 29 shows the disaggregation bar charts corresponding to the fourth IM level.

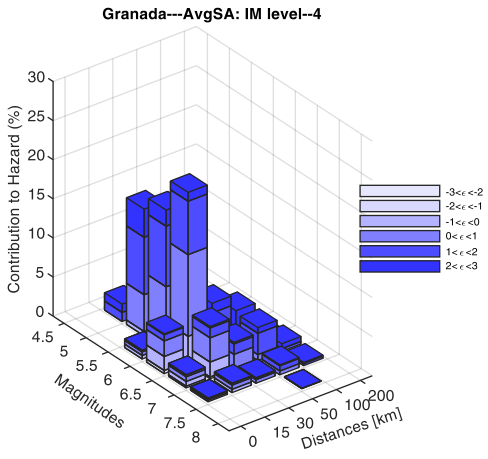

Figure 29. Disaggregation analysis results obtained for a return period of 475 years of AvgSA in Granada.

In each set (or IM level), 21 pairs of records are selected based on the geometric mean of the two horizontal components. The Correlation model of Baker and Jayaram (Baker and Jayaram, 2008) has been used in the selection procedure. During this step the scaling factor has been limited to maximum of 6.0 for all IM levels in order to get the best match.

The records were selected from the NGA-West database (Chiou et al., 2008) and no distinction between pulse-like and non-pulse-like records has been done. Also no limitations for the causal parameters of the selected records in terms of $\overline{M}$, $\bar{R}$ and Vs30 are accounted for in the selection. Figure 30 shows the selected records and 2.5/50/97.5th percentiles of the CS target spectra for the fourth IM Level.

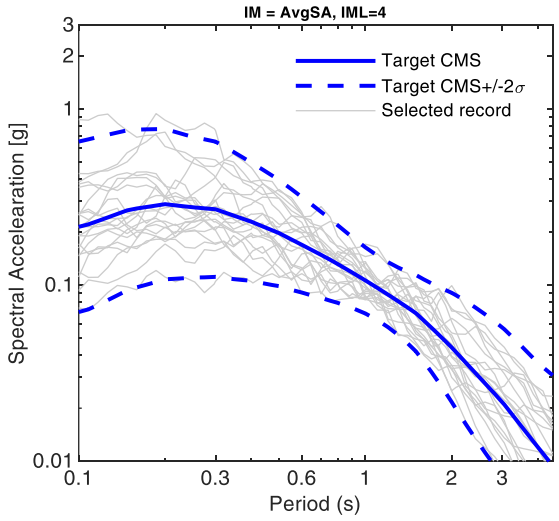

Figure 30. Selected records and the 2.5th/50th/97.5th percentiles for Granada using AvgSA as the conditioning IM corresponding to a return period of 475 years.

6.3 Analysis of results and Fragility Curves

Vulnerability in quantitative terms is defined here by using fragility curves. A Fragility Curve (FC) expresses the conditional probability of reaching or exceeding a certain damage state due to a seismic event of a given intensity.

In this case, a FC is derived from the results obtained from the FE analysis of the degraded and non-degraded models when subjected to seismic event of ten different intensities (see 6.2). The fragility curve is obtained by analysing the response of the numerical model against accelerations introduced at the ground level. The probability of exceedance of a certain value of reference is analysed.

6.3.1 Puerta Elvira

In the case of PE the most noticeable variation in the response of non-degraded and degraded models corresponds to the displacement of the top left corner of the main façade (point P in Figure 23).

In order to establish a reference displacement to build the FC, a push-over static analysis of the FE model in Figure 23 is carried out. Maximum and minimum principal stresses in the element of rammed earth in the extrados of the arch next to the apex as a function of the relative displacement imposed at the top of the arch of PE (see Figure 23) are represented in Figure 31. In Figure 31 the tensile (positive) and compressive (negative) strengths of rammed earth are represented with horizontal lines. As can be seen in Figure 31, the displacement of reference is adopted as the one for which the mean compressive strength of the rammed earth is reached (here, compression is negative).

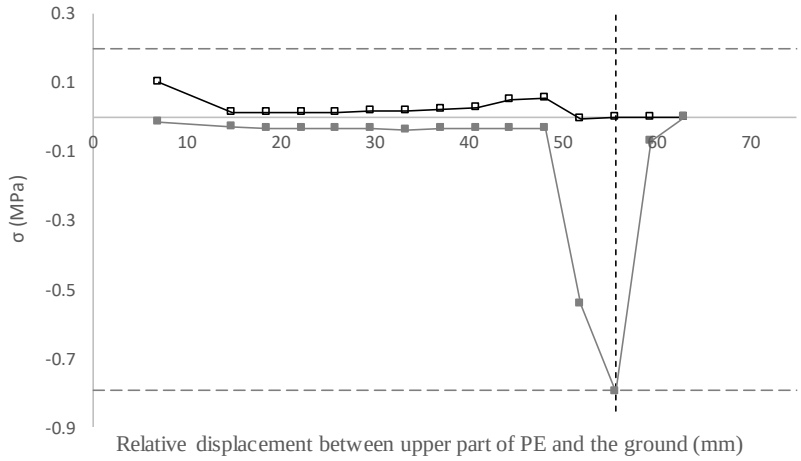

Figure 31. Maximum and minimum principal stresses as a function of the relative displacement imposed between the upper part of the main body of PE for the non-degraded numerical model, see Figure 23. FE push-over static analysis.

The maximum displacements at point P obtained from the numerical analysis for the values of intensity IM considered are represented in Figure 32.

The fragility curves herein are estimated from multiple stripe analysis results obtained from FE analysis considering the artificial earthquakes and following the framework developed by Baker (Baker, 2015). As recommended in (Aschheim, Hernández-Montes and Vamvatsikos, 2019), two stripes differing at least 25% are considered to obtain the fragility curve of PE in the non-degraded state and considering the rectangular mean degradation pattern (Figures 14 and 27).

The corresponding FC is represented in Figure 33. The selected parameter is the displacement of point P assuming damage when this value reaches 55.5 mm (see Figure 31), which corresponds to around L/280. The analytical expression of the fragility curves in Figure 33 are derived using a lognormal cumulative distribution function (Aschheim, Hernández-Montes and Vamvatsikos, 2019; Kim *et al.*, 2021).

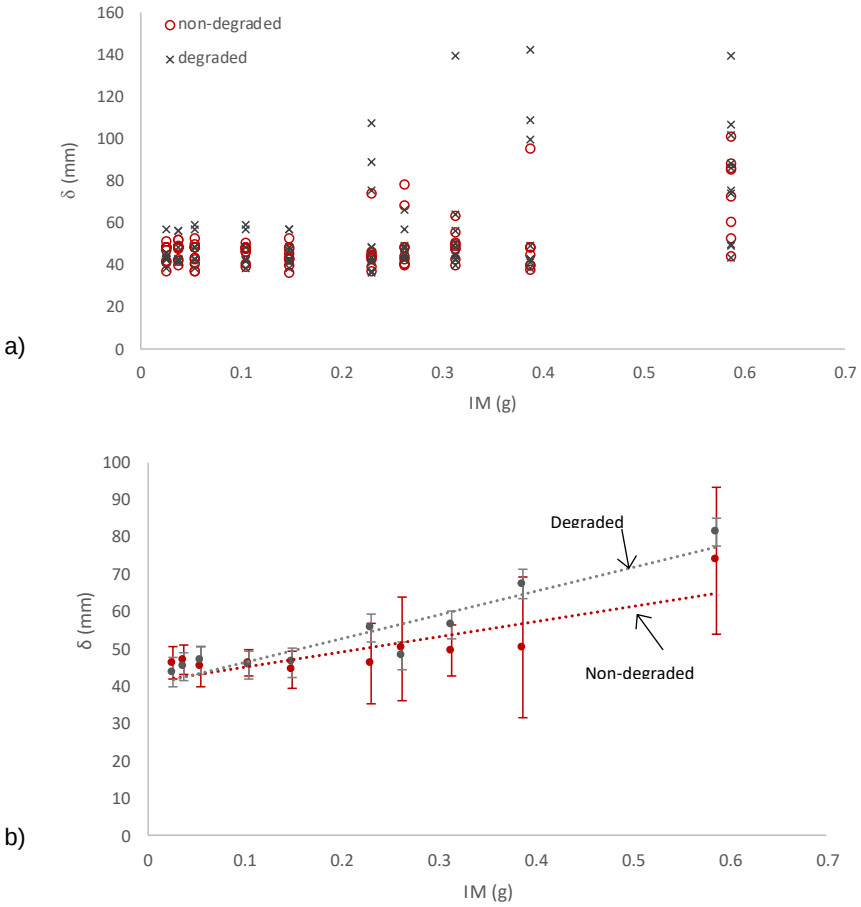

Figure 32. Maximum displacement at point P (Figure 23) from FE seismic analysis. a) Scattered points. b) Mean values, Standard Deviations and trend lines.

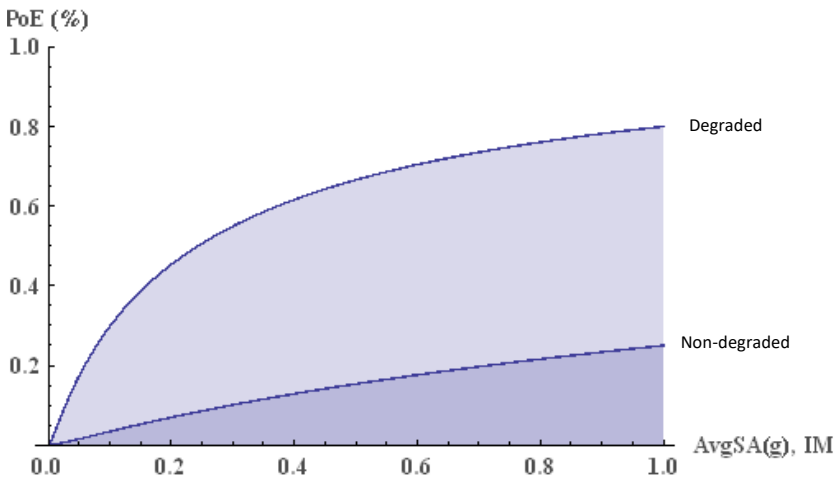

Figure 33. Fragility curve of PE. Reference's parameter: top corner displacement corresponding to L/280.

Figure 33 shows that the PE degradation leads to a less seismically resilient performance over the entire IM range. It can be seen that, for the peak ground acceleration at Granada (0.23g), the level of degradation measured in the Zirid wall would lead to an increasing of around 40% the probability of exceedance of the limit displacement.

6.3.2 Monastery of San Jerónimo

In this case, there is little difference between the top displacements of the tower (point P in Figure 24) of both non-degraded and degraded models, so as reference parameter the minimum principal compression stress is chosen (note that compression is negative). As can be seen in Figure 34, maximum principal tensile stresses are almost zero in all the cases.

For the non-degraded model, the original geometry is chosen. The actual state, 503 years old, is considered for the called degraded model. The OEDP has been applied as a rectangular pattern to the buttresses of the apse and as a triangular shape to the rest of the perimetral wall, see Figure 27.

It is important to note that given the linearity of the procedure, any change in environmental conditions is addressed by a new value of the UCP (Figure 19). Resulting that an increment of t (Δt), with the new UCP, becomes in an increase in deterioration OEDP (ΔOEDP).

Figure 34 shows the minimum compression stresses (compression is negative), mean and standard deviation, in elements A and B (which are the ones with the highest compressive stresses of the numerical model, see Figure 24) for the 10 intensity levels considered.

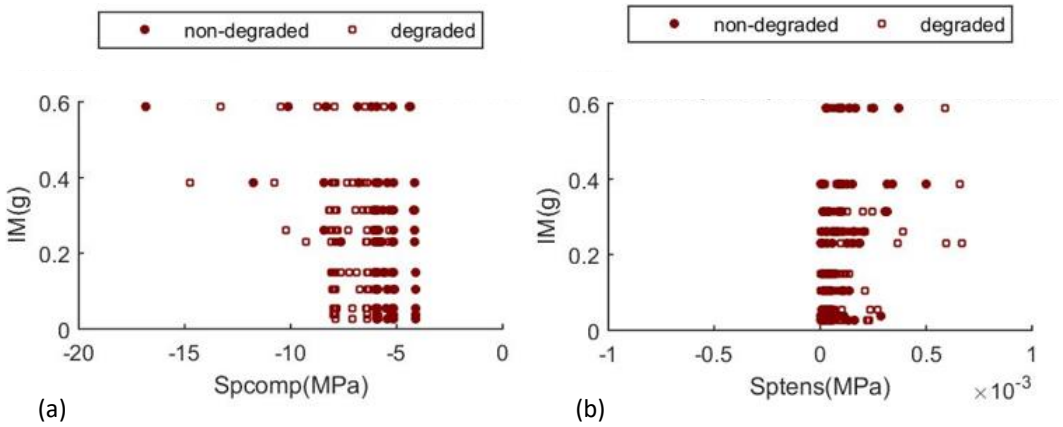

Figure 34. (a) Minimum –compressive- and (b) maximum –tensile- principal stresses from FE seismic analysis.

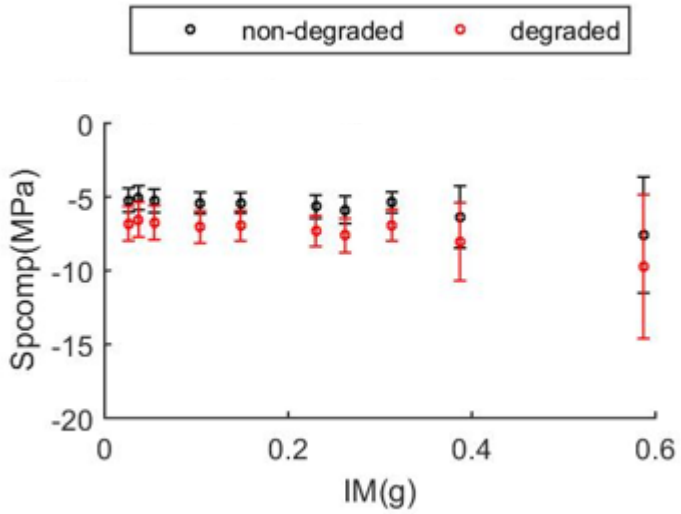

Figure 35. Mean and SD of the minimum compressive principal stresses

The fragility curve is obtained by analysing the response of the numerical model to different intensities. The probability of exceedance of a stress of 8 MPa is analysed (percentile of 95%). This election is done based on the importance of the size effect over the size of the tested specimens (50×50×50 mm). Two stripes differing at least 25% are considered to obtain the fragility curve, in Figure 36.

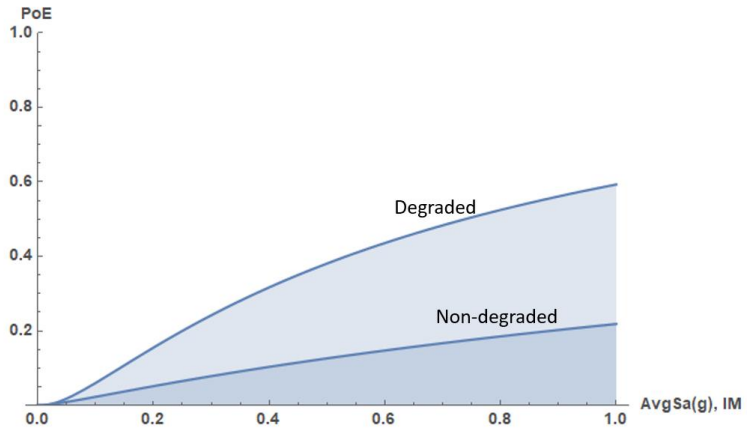

Figure 36. Fragility curve of San Jerónimo. Reference's parameter 8 MPa in the most stressed elements of the Monastery.

As can be seen in the fragility curve, deterioration increases the probability of failure.

7 Analysis of the cost of interventions

A database based on recently executed restoration projects in the study sites (Granada, Rhodes, Venice and Tonsberg) has been created. Among others the rehabilitation of the foundational hospital of the Hospitalarian order of Saint John of God has been analysed (XVI century), a work currently in progress. Rhodes Municipal Theater rehabilitation has also been studied, both works presented similar prices. In this approach, the studied heritage buildings have been divided into three parts: facade, interior slab and roof, see Figure 37.

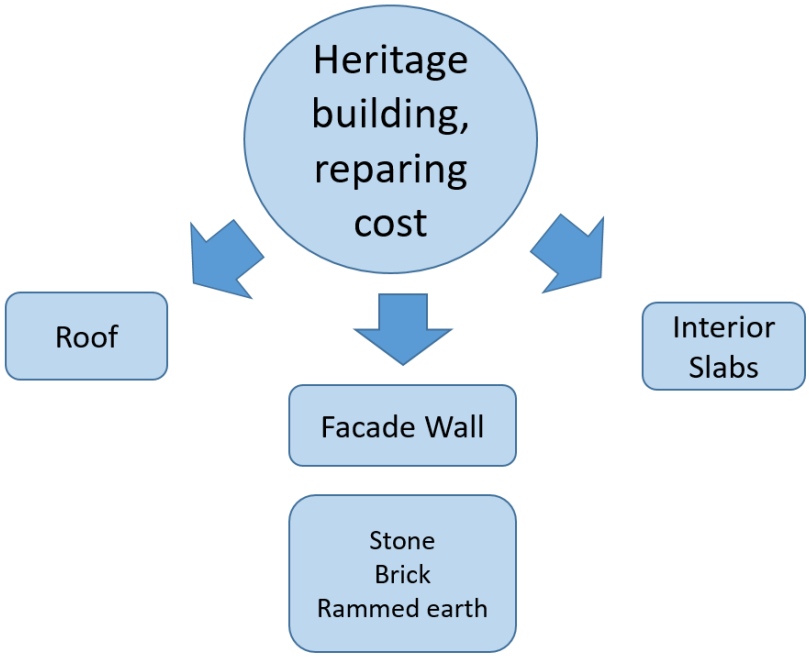

Figure 37. Cost of interventions.

The fundamental objective is to obtain a price list that is operational, faithful to reality and without going into constructive details. See Table 3. In addition to the database, for the preparation of the price list, professionals specialized in the design and execution of restoration works have been used.

Table 3. Cost of interventions pricelist.

Facade Wall			
Brick			
	Repair	200	€/m^2
	New (24 cm thickness)	154	€/m^2
Stone (calcarenite)			
	Cleaning, sanitizing, consolidation, and mortar repair (< 5 cm of degradation)	450	€/m^2
	Stone reposition (additional cost)	1300	€/m^3
Rammed earth			
	Without scaffold	480	€/m^3
	With scaffold	580	€/m^3
Interior Slab			
	Repair of a timber slab	300	€/m^2
	Substitution of a timber slab	175	€/m^2
Roof			
	Historical building (preserving existing parts)	1800	€/m^2
	Regular XVI century building	500	€/m^2
	Full substitution with new timber	400	€/m^2
Installations			
	All installations, including elevator	1850	€/m^2

This table can be used for repairs in Granada and in Rhodes. Due to added difficulties in transport and handling, prices in Venice must be multiplied by 1.4.

7.1 Study case of the Monastery of San Jerónimo

According to the hazard curve (Figure 28), if the age of the Monastery is considered as the mean return period, which corresponds to 9.5% in 50 years, a 0.2g intensity is reached. In this case, the degraded Monastery (actual state) has a probability of exceedance of almost 15% while the probability of exceedance of the non-degraded case is 5%. So, it can be concluded that approximately 10% of the perimeter of the monastery is damaged by typical compression failure. This deterioration can be seen in the buttresses of the apse, which confirm the results obtained from the FC.

Given that an incremental moderate of damage can be expected respect to its actual state, a restoration should prevent future damages. Given the nature of the deterioration observed, a good choice is a 5 cm substitution of the superficial thickness plus 20 cm of additional protection. The restoration should affect the entire perimeter (171 m long) up a height of 1.5 m. The proposed reparation includes cleaning, sanitizing, consolidation and stone reposition. The cost of the reparation, according to the standards used in the area of Granada is around 200 thousand euros.

Bibliography

Krommyda, M. & the HYPERION Consortium (2020). Architecture specification. Deliverable D2.3 URL https://www.hyperion-project.eu/deliverables/

A. Almagro and A. Orihuela (2014) 'Puerta de Elvira (1992) y Cuarto Real de Santo Domingo (2001-2004), Granada', in *La restauración de la tapia en la Península Ibérica: criterios, técnicas, resultados y perspectivas ; coord. por Camilla Mileto, Fernando Vegas López-Manzanares, , ISBN , págs. 236-241*, pp. 236–241.

Almagro, A., Orihuela, A. and Vílchez, C. (1992) *La Puerta de Elvira en Granada y su reciente restauración*.

Aschheim, M., Hernández-Montes, E. and Vamvatsikos, D. (2019) *Design of reinforced concrete buildings for seismic performance: practical deterministic and probabilistic approaches*. CRC Press. Taylor & Francis. Available at: https://www.crcpress.com/Design-of-Reinforced-Concrete-Buildings-for-Seismic-Performance-Practical/Aschheim-Hernandez-Montes-Vamvatsikos/p/book/9780415778817.

Aubert, J. E. *et al.* (2013) 'An earth block with a compressive strength higher than 45 MPa!', *Construction and Building Materials*, 47, pp. 366–369. doi: 10.1016/j.conbuildmat.2013.05.068.

Baker, J. W. (2015) 'Efficient analytical fragility function fitting using dynamic structural analysis', *Earthquake Spectra*, 31(1), pp. 579–599. doi: 10.1193/021113EQS025M.

Baker, J. W. and Cornell, C. A. (2005) 'A vector-valued ground motion intensity measure consisting of spectral acceleration and epsilon', *Earthquake Engineering and Structural Dynamics*, 34(10), pp. 1193–1217. doi: 10.1002/eqe.474.

Baker, J. W. and Jayaram, N. (2008) 'Correlation of spectral acceleration values from NGA ground motion models', *Earthquake Spectra*, 24(1), pp. 299–317. doi: 10.1193/1.2857544.

Bazzurro, P. and Cornell, C. A. (1999) 'Disaggregation of seismic hazard', *Bulletin of the Seismological Society of America*, 89(2), pp. 501–520.

Boore, D. M. and Atkinson, G. M. (2008) 'Ground-motion prediction equations for the average horizontal component of PGA, PGV, and 5%-damped PSA at spectral periods between 0.01 s and 10.0 s', *Earthquake Spectra*, 24(1), pp. 99–138. doi: 10.1193/1.2830434.

Chiou, B. *et al.* (2008) 'NGA project strong-motion database', *Earthquake Spectra*, 24(1), pp. 23–44. doi: 10.1193/1.2894831.

Coletti, C. *et al.* (2016) 'How to face the new industrial challenge of compatible, sustainable brick production: Study of various types of commercially available bricks', *Applied Clay Science*, 124–125, pp. 219–226. doi: 10.1016/j.clay.2016.02.014.

Cultrone, G., Sebastia, E. and Ortega Huertas, M. (2007) 'Durability of masonry systems : A laboratory study', *Construction and Building Materials*, 21, pp. 40–51. doi:

10.1016/j.conbuildmat.2005.07.008.

Ghobadi, M. H. and Torabi-Kaveh, M. (2014) 'Assessing the potential for deterioration of limestones forming Taq-e Bostan monuments under freeze–thaw weathering and karst development', *Environmental Earth Sciences*, 72(12), pp. 5035–5047. doi: 10.1007/s12665-014-3373-8.

Giardini, D., Woessner, J. and Danciu, L. (2013) *Seismic hazard harmonization in Europe (SHARE): online data resource.*

Gil-Martín, L. M., Fernández-Ruíz, M. A. and Hernández-Montes, E. (no date) 'Mechanical characterization and creep behavior of a stone heritage material used in Granada (Spain): Santa Pudia calcarenite', *Rock Mechanics and Rock Engineering*, RMRE-D-21-.

Girardeau-Montaut, D. (2016) 'CloudCompare. Retrieved from CloudCompare: https://www. danielgm. net/cc'.

https://almunecarh.wordpress.com/2013/11/06/granada-ziri-1-puerta-elvira/ (no date).

Jalón, M. L. *et al.* (2020) 'Probabilistic identification of surface recession patterns in heritage buildings based on digital photogrammetry', *Journal of Building Engineering*, 34(October 2020). doi: 10.1016/j.jobe.2020.101922.

K.J. William and E.D. Warnke (1975) 'Constitutive model for the triaxial behaviour of concrete', *Proc of the Int Assoc Bridge Structural Engineering, ISMES, Bergamo*, 19, p. 174.

Kim, J. *et al.* (2021) 'Seismic vulnerability assessment of free-standing massive masonry columns by the 3D Discrete Element Method', *Engineering Structures*, 246(July), p. 113004. doi: 10.1016/j.engstruct.2021.113004.

Lerma, J. L., Cabrelles, M. and Portalés, C. (2011) 'Multitemporal thermal analysis to detect moisture on a building façade', *Construction and Building Materials*, 25(5), pp. 2190–2197. doi: https://doi.org/10.1016/j.conbuildmat.2010.10.007.

Luque, A. *et al.* (2008) 'Effectiveness of stone treatments in enhancing the durability of bioclastic calcarenite in (Granada, Spain)', *Materiales de Construcción*, 58(292), pp. 115–128. doi: 10.3989/mc.2008.41607.

Maravelaki, P. *et al.* (1992) 'Investigations of the Surface Processes on Exposed Limestones', *MRS Proceedings*. 2011/02/28, 267, p. 943. doi: DOI: 10.1557/PROC-267-943.

Melchor, C. (2021) *Patrones de degradación en edificios históricos.Puerta de Elvira (Granada).Master thesis.*

Molina, E. *et al.* (2011) 'The pore system of sedimentary rocks as a key factor in the durability of building materials', *Engineering Geology*, 118(3–4), pp. 110–121. doi: 10.1016/j.enggeo.2011.01.008.

Molina, E. *et al.* (2013) 'Evaluation of stone durability using a combination of

ultrasound, mechanical and accelerated aging tests', *Journal of Geophysics and Engineering*, 10(3). doi: 10.1088/1742-2132/10/3/035003.

Molina Piernas, E. (2015) *Influencia de la textura, del sistema poroso y del acabado superficial en la durabilidad de areniscas y travertino explotados en Andalucía y utilizados en construcción*. University of Granada.

Monelli, D. *et al.* (2012) 'The hazard component of OpenQuake: The calculation engine of the Global Earthquake Model', *15th World Conference on Earthquake Engineering*, (September 2014), p. 8. doi: 10.13140/2.1.3307.1364.

Rodriguez-navarro, C. and Sebastian, E. (1996) 'Role of particulate matter from vehicle exhaust on porous building stones (limestone) sulfation', *The Science of the Total Environment*, 187, pp. 79–91.

Vázquez, P. *et al.* (2013) 'Evaluation of the petrophysical properties of sedimentary building stones in order to establish quality criteria', *Construction and Building Materials*, 41, pp. 868–878. doi: 10.1016/j.conbuildmat.2012.12.026.

Yue, J. *et al.* (2022) 'Study on Deterioration of Gray Brick with Different Moisture Contents under Freeze – Thaw Environment'.